# Auroral Illumination of Solid Bodies

**Charles L. Bennett[1] and Notanee Bourassa[2]**

[1]Retired from Lawrence Livermore National Laboratory, Livermore, CA, USA

[2]Saskatchewan Aurora Hunters, Saskatchewan, Canada

Corresponding author: Charles Bennett (Charlie_Bennett@comcast.net)

**Key Points:**

- The 3-d position and velocity vectors of numerous ionospheric objects are determined by triangulation of images from multiple cameras
- Rapid variation in color and intensity of these objects has been observed and is attributed to auroral bombardment-induced light emission
- Auroral bombardment-induced light emission of meteor dust could provide a physical mechanism for the appearance of STEVE

## Abstract

Numerous objects in the ionosphere, including both satellites and meteors, having rapidly varying light intensity and color have been observed in photographs taken during an active aurora. It is suggested that theses variations may be attributed to Auroral Bombardment-induced Light Emission and Sputtering produced by auroral particles striking these objects. This phenomenon is found to increase the brightness of some objects by more than a thousand-fold. It is hypothesized that this phenomenon acting on a remnant dust cloud from ablated meteoric material left along the path of its trajectory through the ionosphere could produce the optical emissions known as STEVE (Strong Thermal Emission Velocity Enhancement). The July 25, 2016 STEVE event is very closely aligned in 3-dimensional direction with the location of the radiant for the Southern Delta Aquariid meteor shower. The best alignment in time with the radiant direction coincides with the appearance of rising flashes of light that occurred 5 minutes before STEVE's initial visibility. These rising flashes of light might also be caused by the hypothetical meteor.

## Plain Language Summary

Most meteors emit light between 70 and 120 km above the earth from friction while passing through the atmosphere. Higher altitude meteors between 130 to 170 km, where the air is too thin to produce such friction, can become luminous through a different process of thermalization of sputtered particles. The highest known meteor from the Orionid meteor shower became visible at 168 km and its light is attributed to this process.

In this article, we suggest that the bombardment of high-altitude solid bodies, such as space junk, artificial satellites and comet or meteor dust, by concurrent auroral activity generates sufficient light that otherwise invisible objects may be readily seen with widely available digital cameras. We have found several examples of this process, including one meteor at a height of nearly 1,000 km above the earth's surface.

We also find that light emission along long linear trails in the ionosphere can be explained as auroral bombardment-induced light emission from the remnant dust from a meteor.

Auroral bombardment-induced light emission of the large number of existing high-altitude bodies could open up an entirely new window for a better understanding of these bodies, the aurora, and the ionosphere.


# 1 Introduction

Aurora are well known to be the result of precipitating electrons or protons exciting atmospheric atoms and molecules whose subsequent decay produces visible light. To the best of the author's knowledge, it does not seem to have been previously noted that auroral bombardment of solid bodies may produce light of sufficient intensity to be readily detected with ground-based cameras and sputtered electrons of sufficient flux to be detectable in the opposite hemisphere. It has been suggested by (Vinkovic, 2007) and (K.A. Hill, 2004) that meteors such as those discussed in (Y. Fujiwara, 1998) and (A. Olech, 2013) too high to produce light by conventional ablation processes could produce detectable light by a sputtering process, but the role of the aurora as an enhancement of this process was not considered. Here evidence is presented that the passage of solid objects through regions of even sub-visual auroral precipitation is correlated with enhanced (sometimes by 3 orders of magnitude) visible

emissions. We will refer to this phenomenon as Auroral Bombardment-induced Light Emission and Sputtering (ABLES). It is hypothesized that solid particles in the dust trail of a meteor or in comet debris may also be illuminated by ABLES from concurrent auroral particles if the dust is high enough to be exposed to auroral bombardment. One such event may have occurred on July 25, 2016 and this case will be the primary focus of this paper.

This event is one example of the thin, east-west-aligned purple-colored aurora-like structure called a "proton arc" or sometimes "Steve" by auroral photographers. This event was associated with sub-auroral ion drift (SAID) by (E. A. MacDonald, 2018) on the basis of data from a satellite that passed over the region of this structure, and this and similar events were given the backronym "Strong Thermal Emission Velocity Enhancement" (STEVE) because of this correlation. The "velocity enhancement" refers to a westward ion flow in excess of 5 km/s in the plasma that the satellite passed through. More recently, (W.E. Archer, 2019) has shown STEVE events to be consistently associated with SAID and in the July 25 case, the Positive Field-Aligned Current was measured to be approximately 500 $nA/m^2$ and extended over approximately 0.7° magnetic latitude. The (D. Lummerzheim, 2001) analysis of an April 11, 1997 SAID event having Red-line intensity at a level similar to our July 25 event, found that the positive FAC was from a flux of precipitating protons with an energy spectrum extending to at least 32 keV (the upper limit of their detector). A tomographic inversion provided the altitude profile of visible emissions in that case. No STEVE structures were seen in the April 11 SAID event.

In (B. Gallardo-Lacourt, 2018) particle data was presented for a STEVE event from March 28, 2008 that was crossed by the POES satellite, and these authors state "We assert that such low precipitating energy fluxes (for protons and especially for electrons) cannot be responsible for the luminosity observed in STEVE". These authors, however, did not consider the possible enhancement of luminosity from ABLES. In (B. Gallarod-Lacourt, 2018) a statistical analysis of 28 STEVE events finds that they have a latitudinal width only ¼ the width of narrow auroral structures, and typically have an equatorward displacement of about 50 km over the course of an average duration of 1 hour. It is not explained how the average equatorward drift velocity <0.02 km/s is compatible with the "velocity enhancement" of 5 km/s in the westerly direction. It is also not explained why the latitudinal width of STEVE is so much less than the auroral structures.

(D.M. Gillies, 2019) presents spectroscopic observations of the April 10, 2018 STEVE event that reveals the green picket fence structure to be associated with a strong OI (557.7 nm) emission similar to emissions produced in typical aurora. The narrow purple structure was found to have a broad continuous spectrum, with some OI red-line (630 and 636 nm) emission. These authors state "The above observations essentially exclude STEVE from being an auroral phenomenon". They conclude that the "elevated electron temperature" associated with the purple STEVE features would produce "thermal emission" of the red-line structure.

(Y. Nishimura, 2019) showed that the May 8, 2016 STEVE event having a green picket fence structure in photographs taken from the ground in the northern hemisphere showed a conjugate structure in the southern hemisphere. These authors state "The subauroral precipitation structure and upward FAC are strikingly different from typical SAID events". These authors also find that the April 12, 2008 event without a picket fence structure did not show a conjugate structure in the opposite hemisphere and did not show the "strikingly different" upward FAC.

Here we list several hitherto unanswered questions about STEVE events in general, and some concerning the 2016-7-25 STEVE event in particular that we will quantitatively answer in the following. Why is STEVE visible, while most SAID events are not associated with optical emission? Why is the width of this STEVE (0.15° MLAT) much less than the width (1° to 2° MLAT) of typical SAID events? Why is the green picket fence structure also very narrow and aligned with the narrow purple streaks in magnetic latitude and longitude? Why is the green picket fence at a nearly constant low altitude, while the narrow purple band initially has a linear decrease in altitude along its longitudinal extent? Why are conjugate STEVE structures seen in the opposite hemisphere for events with green picket fence features, but not in events without these features? What accounts for the "strikingly different" upward FAC in the STEVE event with a conjugate structure in the opposite hemisphere? What can account for the purple color of the upper portion of STEVE? While the 7-25 SAID event displayed up to 5 km/s of westward ion motion, why did this STEVE structure drift westward at a speed of no more than 0.05 km/s?

Our hypothesis of a remnant dust trail produced by a meteor from the Southern Delta Aquariid (SDA) shower with ABLES answers all of these questions. In the following, we present observational evidence that the 3-dimensional location and character of the luminosity from the July 25 STEVE event can be explained by 2 components. One being the time the SDA meteor struck, and the second being the location in 3-d space of the perigee of this meteors orbit. We will present observational evidence that both of these components are unambiguously determined directly from the data.

In preparation for the discussion of our hypothesis for the July 25 STEVE event, we first present observational evidence, based on the analysis of the brightness distribution in 3-d space and time of several earth orbiting satellites that makes the case for the reality of ABLES, and the thousand-fold gain in brightness of solid objects that can be produced by auroral bombardment.

In section 3 we primarily focus on the observational data. In section 4 we briefly discuss the well-known phenomenon of Bombardment-induced Light Emission (BLE) and introduce our Auroral BLE and Sputtering (ABLES) concept. In section 5 we turn to our hypothesis for STEVE and how this hypothesis answers the questions posed in the introduction. In section 6 we discuss how ABLES can provide a new window for a better understanding of the large number of ionospheric solid bodies, the aurora, and the ionosphere.

## 2 July 25, 2016 Observations

This STEVE event was photographed by N. Bourassa from a site near Regina Saskatchewan (REGI). Concurrent with the photographs published in (E. A. MacDonald, 2018), a number of All Sky Imager (ASI) images were recorded, including from sites at Lucky Lake (LUCK) in Saskatchewan, Athabasca (ATHA) in Alberta and The Pas (TPAS) in Manitoba. The complete sequence of images from the ASI cameras are available for download from (University of Calgary, 2018). The details on the spatial resolution, spectral coverage and site location for these various cameras are tabulated in Table 1 in the supplemental materials.

To exploit parallax effects between cameras, pixels in each image were registered to local angular coordinates of azimuth and altitude using a number of stars in the images. The reference stars locations and magnitudes were taken from the Yale bright star catalog (Hoffleit, 2014). For the REGI camera a primarily gnomonic projection (Weisstein, 2109) was used. For the ASI cameras with fisheye lenses, a primarily linear equidistant projection (Bettonvil, 2005) was used.

For both types of lenses, correction for barrel distortion was required to provide acceptable registration. The details of this process are provided in the text file, including the Matlab (Mathworks, 2019) functions used, available in the supplemental materials.

# 3 Observations of satellites, meteors and STEVE

Within a series of REGI photographs of STEVE spanning a period of 18 minutes, 31 transient streak events were observed in more than 1 frame. The altitude for most of these could not be determined, as no corresponding transient streak could be detected in any other ASI camera by virtue of their much lower sensitivity level of approximately magnitude 3.5 for 10 coadded frames vs. magnitude 11 for each of the REGI RGB colors in a single frame (see Table 1). However, 6 of these objects were also observed in at least one frame of at least one ASI camera and were determined to be high-altitude objects. These objects are numbered in terms of their order of appearance. Object-6, the brightest, was seen in all 4 imagers. In addition to these multi-frame objects one extended transient event was seen in a single frame in both LUCK and REGI and from its brightness profile, altitude and speed is identified as a meteor.

A pair of transient events not included in the count of 31 above could be identified as aircraft, by virtue of the regular blinking of the light at a frequency between 40 and 100 flashes per minute associated with the anti-collision light system required for aircraft. One of these had a color consistent with “aviation red” while the other was consistent with “aviation white”. These aircraft are identified in the relevant movie files included in the supplemental materials.

## 3.1 Object-2 Example

Object-2 was seen by 2 of the 4 imagers over multiple successive frames. This object appears as linear streaks in 20 successive REGI images at 8.34 s intervals with the locations of the leading end of each streak marked by the 19 green circles and single white circle in figure 1. The white circle indicates the last location of the object and direction of travel as it exits the REGI camera field of view. This object also appears as shorter streaks in 6 LUCK images taken at 3s intervals. The images from LUCK and REGI at the time of greatest intensity are displayed in figure 1. The registered images are identified by the 4-letter abbreviation for each site, together with the UTC time at the end of the exposure of the specific image. In each image, the large cyan circle indicates the position of the local horizon. In all images, North is at the top and West is to the right. In the LUCK image, the brightness of this object is comparable to the bright stars Vega and Arcturus. This object is not detected in any of the TPAS or ATHA (grayscale) images, despite the clear visibility of Vega and Arcturus in these images. The greater brightness of object-2 in the LUCK image relative to TPAS and ATHA is attributed to the presence of a strong spectral line in the 630 nm LUCK passband (Jun Liang, 2016) for this object.

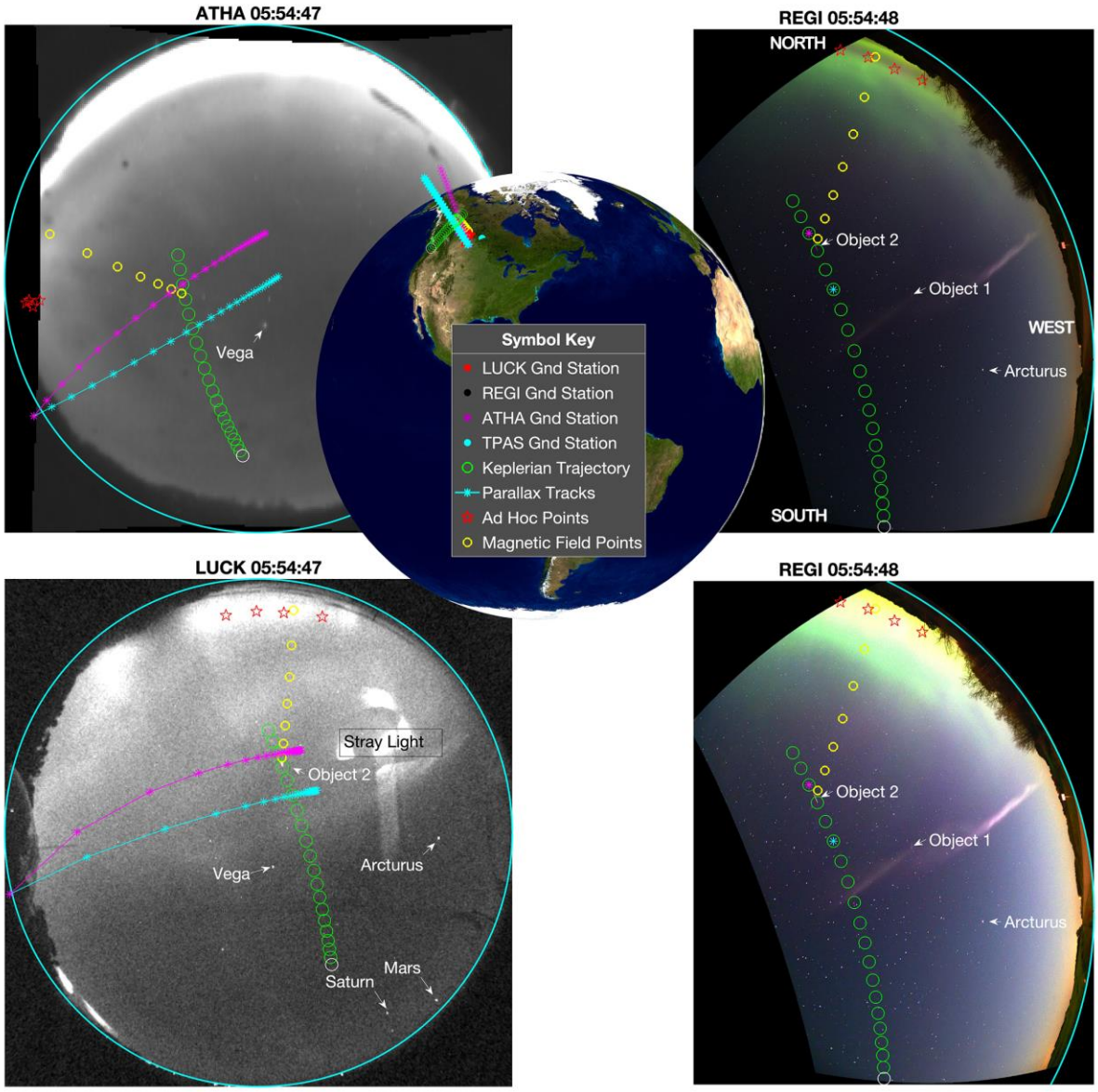


Figure 1. An example illustrating the use of parallax to determine altitude.

A particular point of interest, such as that marked by the magenta asterisk in the REGI image in the center of the 3rd green circle from the top of the image, corresponds to specific azimuthal and elevation angles from the REGI point of view. This particular point will appear somewhere along a curve in the other imagers, with the location determined by the altitude of the point. Representative locations, spaced at 100 km intervals along the line of sight extending from the camera at the REGI site in the direction corresponding to the magenta asterisk in the REGI image, are indicated by the magenta asterisks shown superimposed on the images from the other imagers, as well as over the surface of the globe at the center of the figure. These are labeled "Parallax Tracks". The magenta asterisks in each image are joined by magenta line segments. The altitude of the magenta asterisk point in the REGI image is determined by the intersection of the magenta parallax track with the observed trajectory of object 2 in the LUCK image.

Similarly, the cyan asterisks linked by cyan line segments represent the line of sight corresponding to the center of the 6th green circle from the top in the REGI image. Just as for the magenta case, the altitude of the cyan asterisk in the REGI image is determined by the intersection of the cyan parallax track with the trajectory seen in the LUCK imager. Parallax tracks are extremely helpful in the process of altitude determination but for clarity are not always shown in later figures.

Synchronization of the REGI and LUCK clocks can be obtained from the position of the light streaks seen in both imagers. As the leading end of the object 2 streak is approximately 1/8 of the inter-circle distance above the center of the 4th green circle in the LUCK image, the exposure of the LUCK image shown terminated approximately 1 s before the exposure of the REGI image shown. The LUCK recorded times were taken as the reference. The REGI times as recorded in the metadata for each photograph needed to be adjusted by subtraction of 163 seconds. The ATHA recorded times required subtraction of 24 seconds, while the TPAS recorded times required subtraction of 14 seconds. With the altitude of the green circles between the magenta and cyan parallax tracks determined, the 3-dimensional position and velocity vectors can be determined using any pair of successive points. It is found that all 20 of the REGI positions along the trajectory of object-2 are consistent with a Keplerian orbit, having an altitude at the magenta point of 737 km, and a speed of 9.0 km/s. As this speed is significantly less than the escape velocity for this altitude of 10.3 km/s, this object is in a gravitationally bound orbit about the earth, and thus this object is identified as a satellite in Low Earth Orbit (LEO). The rotation of the earth underneath the Keplerian trajectory must be accounted for in order to yield the correct positions in the other REGI images.

Four “Ad Hoc” points marked by red pentagrams along the distinct edge of the green aurora at the northern end of the REGI image (best seen in the REGI image in the upper right hand corner of the figure displayed with an expanded intensity range) are used to determine the magnetic latitude of that aurora as discussed further in section 3.5 below. The magnetic field was computed with the POMME code (CIRES, 2019) using parameters reflecting the state of the magnetosphere at the time of the image. The specific magnetic field line that passes through the trajectory of Object-2 near its point of greatest brightness is shown by the series of yellow circles. The circles mark points along the magnetic field line at altitudes in steps of 100 km along the field line starting from 100 km up to 700 km. It is found that the field line passing through the trajectory of Object-2 at its brightest position also passes through the auroral sheet marked by the red pentagrams.

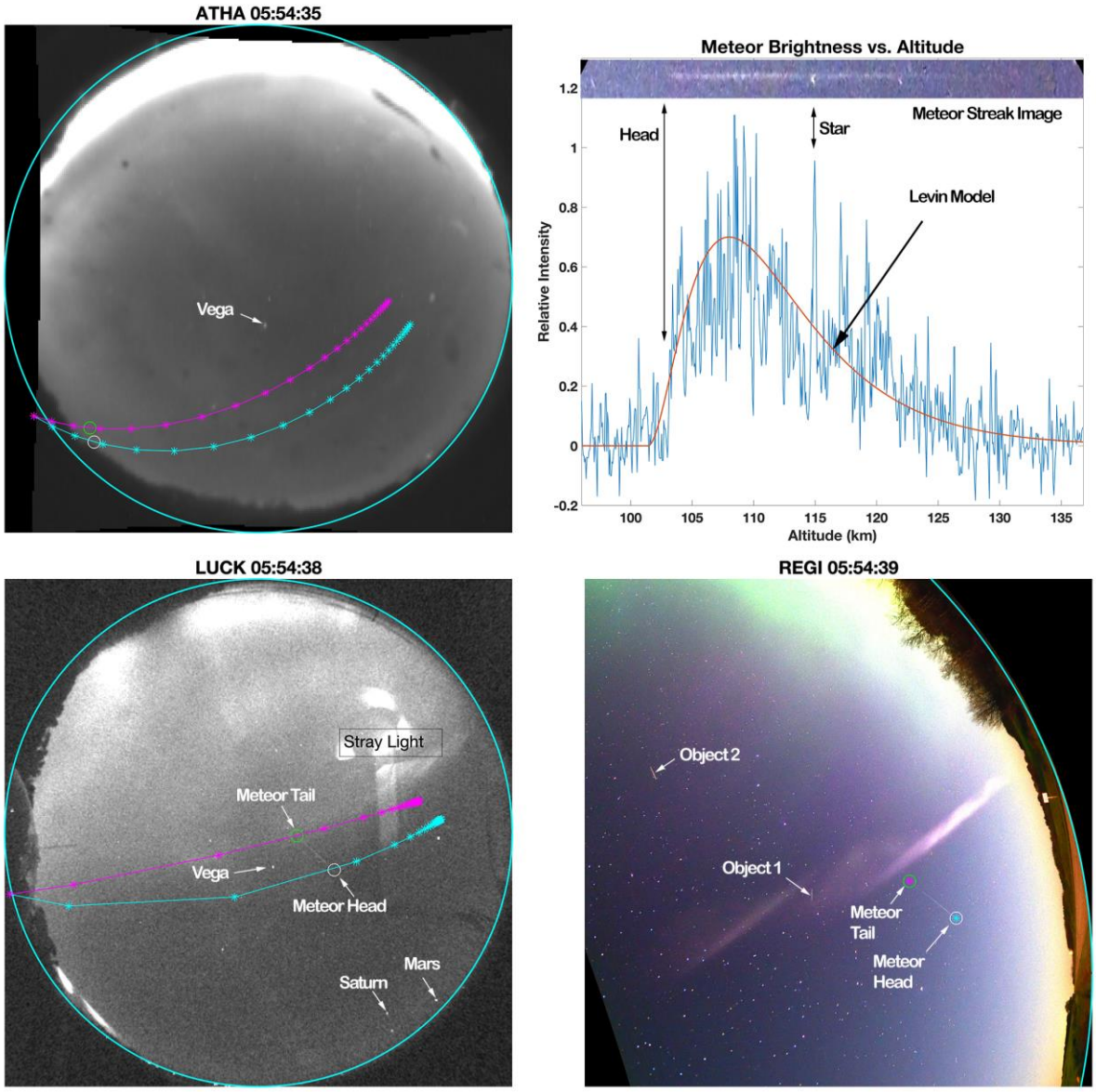


Figure 2. An example illustrating the use of parallax to determine meteor trajectory.

## 3.2 Meteor Case

The LUCK and REGI images shown in figure 2 show an example of a single frame transient event. The brightness of this object varies along its length just as expected for a typical unfragmented meteor. In the upper right corner of figure 2, the plot of the grayscale brightness of this meteor extracted from the REGI image is compared to the model of (Levin, 1963) for the case of a spherical body shown by the red curve. In the top portion of this plot, the region of the REGI image containing this meteor is shown in a narrow strip that is aligned with the intensity plot immediately below it, with arrows indicating the position of a star that happened to lie along the meteor streak. Since the meteor trail extends the full distance between the parallax tracks superimposed on the LUCK image, it can be concluded that the meteor light occurred entirely within the 2 s LUCK camera exposure. This allows a lower bound of 20.3 km/s to be placed on the meteor speed.

In the REGI image shown, objects-1, -2, and the meteor are all simultaneously visible, with an enormously large range of altitudes. The conventional approach of mapping ASI data to a single altitude is hopelessly inadequate for the analysis of such images. In contrast, the approach described here involving the use of "parallax tracks" works quite well, provided clear points of interest can be identified in nearly simultaneous images taken from at least 2 sites at different locations.

### 3.3 Brightness Variations of Streaks as a Function of Time and Position

For both object-1 and object-2 the observed streaks in the REGI images are spread out by their motion over approximately 130 pixels in the original photographs. By virtue of the high resolution and high signal to noise ratio of the REGI data, the variation of the observed intensity along the length of the individual streaks of light in each REGI frame can be usefully converted to a variation as a function of time. The single pixel temporal width obtained is approximately 30ms. The time varying intensities for each of the 3 colors in the REGI data are plotted in the upper section of figure 3. The width of the peaks corresponds to the 4 s exposure for each frame, while the spacing of peaks corresponds to the 8.34 s period between frames. The observed intensities were converted to apparent magnitude using known stars as references. One example is the star β Corona Borealis shown in the small vignette taken from the frame corresponding to the greatest observed intensity for object-1 as indicated by the double arrow. The tilted donut shape of the star image is typical of the stars seen in this portion of this particular photograph and is due to a lack of perfect focus in this image. This blurring also reduces the temporal resolution and is the reason for the slanted edge of the streak at either of its ends. At its brightest, object-1 is over 1,000 times brighter than the threshold of detection at the background level.

The rapid variations in intensity and color observed for both object-1 and object-2 are not consistent with blackbody thermal emission. They may be consistent with ABLES, as will be discussed further below.

The brightness of all 6 objects are displayed as a function of magnetic latitude in the lower left of figure 3. The relative brightness along the trajectory for each object is indicated by the relative sizes of the circles in the lower right. The circle centers correspond to the locations of the leading end of each streak in successive images. The Keplerian orbital parameters that best fit the observations of each object are shown in the legend. Object-1 was observed in 24 REGI frames, but not in either ATHA or TPAS. There were 2 possible streaks seen in 2 different LUCK frames corresponding to 2 different altitudes, and it is also possible that it was low enough to be below the horizon in the other imagers, so its actual altitude is uncertain. Nonetheless, the estimated magnetic latitude distribution shown for object-1, based on the assumption of an altitude of 700km is probably good to within 1° regardless of its exact altitude. Object-3 was observed in 28 REGI frames for one pointing of the camera, and in an additional 24 frames for a second pointing of the camera. It was also observed in ATHA for over 40 frames. Object-4 was observed in 10 REGI frames, but only a single LUCK frame. Thus only a single altitude can be determined, but the slope of this object's trajectory cannot be determined, so its speed is uncertain. Object-5 was observed in 9 REGI frames for one pointing of the camera, and in an additional pair of REGI observations (the northernmost 2 points in the plot) for a different pointing. Object-5 was seen in 63 TPAS frames spanning a greater time range than the REGI observations but was not seen in ATHA and was only seen in LUCK for 22 frames. Object-6 was seen in 50 TPAS frames and 34 REGI frames (at 2 second intervals from the REGI.MOV frames). It is also seen in 18 ATHA frames and 28 LUCK frames. The plotted circles for object-

6 were at 3 s intervals, as it was seen over the longest period of time in the TPAS imager. The brightness for all other objects plotted were taken from the REGI imager at 8.34 s intervals. In all cases, the intensities plotted have been corrected for the effects of range assuming an inverse square law, so that a constant brightness would plot at a constant level independent of range.

The peak brightness of object-2 coincides with its crossing the auroral sheet located at 62° magnetic latitude and whose lower edge is indicated in figure 1 by the 4 red pentagrams. In contrast, no other object has such a peak in brightness as it crosses this same region of magnetic latitude. Objects -1, -4 and -6 instead have brightness peaks at 58.5°±1°, while object-2 also shows a weak secondary peak in brightness near there while its brightness is too low to be detectable between 58° and 60.6°. Object-4 is not even detectable at 62°, despite being well within the field of view of the REGI camera. Objects -3 and -5 do not have brightness peaks within the field of view of the REGI camera. Also, despite being well within the field of view of the REGI and/or ASI cameras, objects -2, -4 and -6 have a brightness too low to be detected at latitudes below 56°.

The brightness peak near 62° in magnetic latitude is clearly associated with the electron aurora seen simultaneously in the REGI photographs. The brightness peak at 58.5°, on the other hand, has no significant visible manifestation in the REGI photographs. It is thus most probably the result of a secondary peak in the sub-auroral proton flux of much less intensity than the concurrent super-auroral proton flux observed in the FESO data. This presumed distribution of proton and electron fluxes is similar to that observed in the proton auroral event discussed by (D. Lummerzheim, 2001) in which Tomographic Imaging was done and an altitude profile of emissions along a magnetic meridian was extracted. In the Lummerzheim work, the 2:45 pass of the DMSP satellite revealed a strong proton flux poleward of the primary electron flux, with a weaker proton flux peak equatorward of the primary electron flux. This electron and proton flux distribution is apparently similar to that seen on July 25, 2016.

The 1.5° width of the brightness peak at 58.5° in figure 3 is typical of the width and location of SAID events (E. Mishin, 2017). In our data, the existence of this sub-auroral proton flux is revealed by the sensitivity “magnification” provided by ABLES acting on objects passing through the region of proton bombardment.

In the legend for the plots in the lower half of the figure, vignettes for all 6 objects are shown to the left of each objects’ respective entry. The right column of vignettes corresponds to the appearance of the objects while they are within the proton flux region. The left-hand vignette column has a single row corresponding to the appearance of object-2 in the electron flux region.

Also shown in the lower right of figure 3 are 3 examples of the location of STEVE ranging from the earliest to the latest times for which concurrent REGI, LUCK and ATHA data are available. The latitudinal distribution of STEVE is confined to the same region as the sub-auroral proton flux. The width of the bars shown for STEVE are not uncertainties in position but rather represent the latitudinal width 0.15° of the observed light distribution at any given longitude. This width is an order of magnitude narrower than the latitudinal width of typical SAID events. The drift in the STEVE location over the course of time could be entirely southward, entirely westward, or a mixture of both. Between 5:50 and 6:34 if the location of STEVE seen in figure 3 is associated with an equatorward drift rather than a westward drift, the latitude decreases by approximately 0.37° in 44 minutes. This corresponds to a speed of no more than 20 m/s in the latitudinal direction. On the other hand, if the drift is purely westward, the longitudinal location changes approximately 5° in 44 minutes corresponding to a drift speed of approximately 100 m/s in the longitudinal direction. This later speed is roughly that of the

neutral wind speeds discussed by (G. Liu, 2013), but it is nearly 2 orders of magnitude less than the 5 m/s SAID flow speed measured by (E. A. MacDonald, 2018).

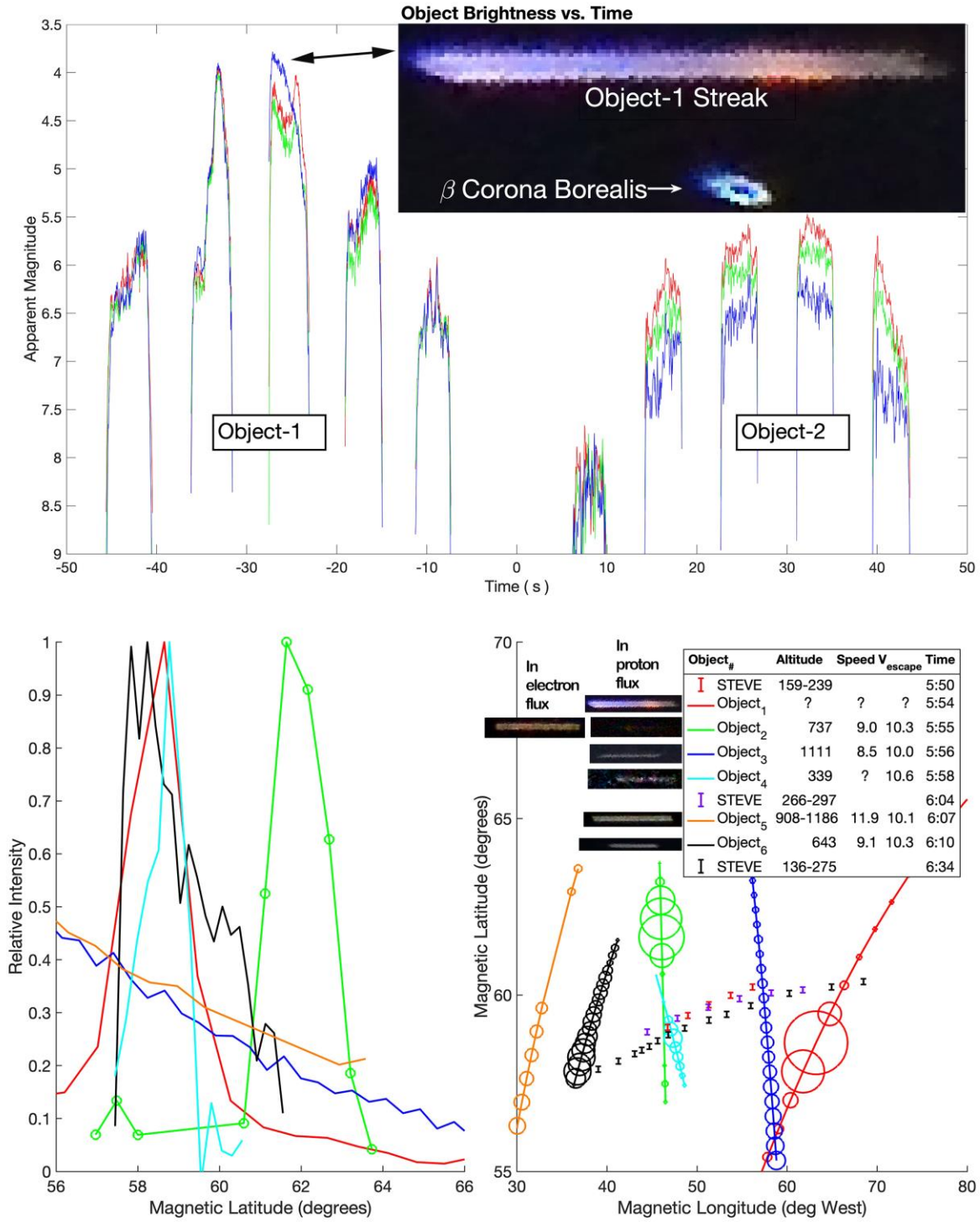


Figure 3. Object brightness is plotted as a function of time (upper half) and location (lower half) in this figure. The location of STEVE emission is plotted with error bars representing the width of the observed emission.

### 3.4 Object Identifications

Objects -2, -3 and -6 are identified as satellites, as their speeds are less than the escape velocity for their measured altitudes. As the speed of object-5 was greater than the escape velocity this object is identified as a meteor. Because of the uncertainty in its altitude and speed, object-1 cannot be identified as either a meteor or satellite. Because of the uncertainty in its speed, object-4 cannot be identified as either a meteor or satellite. Object-3 is tentatively identified as NORAD satellite number 25876, based on the proximity in space and time of the Keplerian orbit computed from the archived orbital elements from (Kelso, 2019) to the observed trajectory.

The object discussed in figure 2 has a brightness distribution entirely consistent with a typical meteor trail. Because it is seen in only a single frame in both the LUCK and REGI cameras, only a lower bound on its speed of 20.3 km/s can be derived. As its speed is above the escape velocity, and its intensity distribution appears meteoric, it is identified as a meteor. In the 3600 LUCK frames between 5:00 and 8:00, this is the only conventional meteor trail found. It may not be merely coincidence that this meteor trail happens to lie within the 58.5°±1° region corresponding to the lower latitude brightness peak. It could be that its luminosity was enhanced by ABLES.

### 3.5 Auroral Imaging Case and Magnetic Field Line Identification

An example of the 3-dimensional analysis of auroral features is shown in figure 4. Here a series of 11 “Ad Hoc” points indicated by red pentagram markers are chosen along the ridge of the very bright auroral structure visible in the TPAS image shown. The displayed intensity range for the TPAS image is chosen to avoid saturation in the image. In the REGI image of this auroral activity, the lower edge of the aurora is quite clear cut, and a precise altitude for the pentagram points can be determined by comparison of the REGI and TPAS images. The altitudes and locations for the 11 points are indicated in the bottom of the figure.

Magnetic field lines passing through each of these points are shown in the figure by blue lines with diamond milestones at altitude intervals of 100 km. The magnetic field lines shown start from a geodetic altitude of 0 km and extend to a maximum altitude of 1,000 km. The POMME code values for the magnetic field are valid to at least 2,000 km in altitude, and well beyond the 1,000 maximum altitude shown here. Note that the positions of the red pentagrams relative to the 100 km altitude milestones along the various magnetic field lines vary as expected for the general increase in the altitude of the edge of the aurora going from east to west across the image.

At the time of this data, the aurora was almost directly over the TPAS imager, and the point of view is staring almost directly up along the local magnetic field lines indicated. The “thickness” of the sheet of auroral activity can be most clearly seen from this end-on perspective, and it is found in places to be only 2 km even while extending over 100km in altitude. A rather complex structure of folds is seen. This structure is dynamic, varying significantly from minute to minute, although the minimum altitude doesn’t vary significantly on this time scale.

The REGI image shows that the green auroral fine structure is closely aligned with the magnetic field lines. This is most clearly seen at the eastern side, with smaller linear structures appearing within the overall green band. The green auroral structure seen in the REGI image is presumably produced by precipitating electrons. From the altitude of the bottom of the green emission it seems that the electron energies were approximately at the 10 keV level, based on typical auroral transport models (Solomon, 2001), but with a significant variation in the energy

of the precipitating particles along the edge of the auroral structure based on the variation in minimum altitude. At the time of this image, with the triangulation of the red pentagram points, the magnetic field lines lead to a value for the magnetic latitude of the green auroral features of 62.15°±0.20°. Over time, the latitude of the green auroral features is seen to vary somewhat.

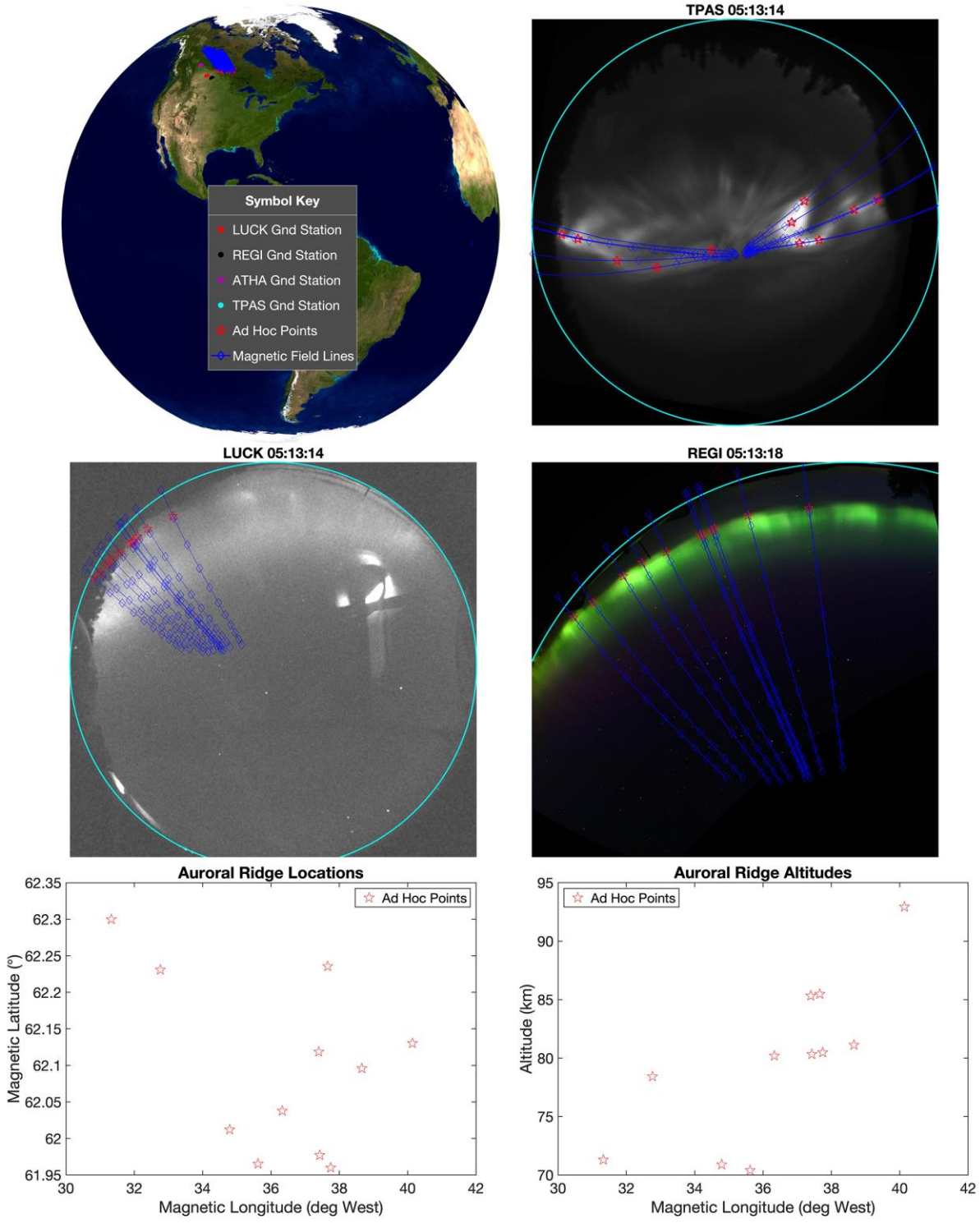


Figure 4. The auroral structure is illustrated.

In order to account for the variation in magnetic latitude of the electron aurora, in images containing visible green auroral sheets, but without a corresponding view from a second site to determine the altitude, it was assumed that the lower edge of the auroral sheets was at the mean altitude determined in figure 4. As an example, the red pentagram "Ad Hoc" points shown in figure 1 were taken to have altitudes of 80±10km, corresponding to the altitude range of the auroral edge observed found for figure 4. With this altitude range, it was found that the magnetic latitude of the green auroral feature at the time shown in figure 1 was approximately 61.8°±0.3°. This is consistent with the location of the brightness peak seen for object-2 as shown in figure 3.

### 3.6 STEVE

The earliest appearance of STEVE is best shown by the difference image of the LUCK data shown in the figure 5. Here, to enhance contrast, 20 images spanning 5:46:32 to 5:47:29 were coadded and the sum of 20 images spanning 5:45:32 to 5:46:29 subtracted. This time corresponds to the earliest onset of STEVE and reveals a highly linear structure that points toward the radiant indicated by the red asterisk (labeled SDA@5:41) for the Southern Delta Aquariid (SDA) meteor shower that was going on at the time. The position of the SDA radiant an hour later is indicated by the second red asterisk (labeled SDA@6:41). The alignment of the linear structure with the SDA@5:41 direction in 3-dimensions is confirmed by the fact that the Keplerian trajectory aligned with this structure asymptotically approaches the location of the SDA@5:41 point in the LUCK image.

At 5:41 a moving light is seen in the ATHA data. The motion of this light can be seen in one of the movies in the supplemental materials. In this movie the trajectory of an object following a Keplerian trajectory is superposed for context. The motion of the moving light approximately follows the local magnetic field lines indicated by the 4 yellow magnetic field points whose coordinates are shown in the lower plots. These same 4 magnetic field points are also shown in one of the movies. The Keplerian trajectory shown is assumed to have its perigee at the location of the earliest appearance of the moving lights in the ATHA camera data as indicated in figure 5. The speed for this trajectory is assumed to be 42 km/s as typical for SDA meteors. The direction of the trajectory at perigee is determined by requiring alignment with the direction to the SDA radiant in 3-d space at 5:41. The altitude at perigee is determined using the earliest available REGI image in conjunction with the 5:41 ATHA image shown.

The earliest available REGI image at 5:48:09 showing STEVE was taken 97 seconds after the 5:46:32 LUCK image. The light seen in the ATHA images to be moving up along the magnetic field lines appears to have left a luminous residue of sufficient intensity to be seen in this REGI image, but not in the 5:46 LUCK, ATHA or TPAS images. This luminous residue is seen in the REGI images to gradually fade over the next several minutes, but to not significantly change in location. By identifying this luminous streak at 5:48 with residue from the moving light seen in the ATHA data at 5:41 that is made visible in REGI by ABLES, the location of the magnetic footprint coordinates of the yellow circles are determined, as well as the altitude of the perigee of the Keplerian trajectory. The yellow circles indicating points along this particular magnetic field line are seen to closely follow the bright streak in the REGI image. The green circles indicating the 3-d Keplerian trajectory shown are at 2.5 s time intervals. That the brighter streak along the magnetic field lines in the REGI image is not seen in the LUCK image can be attributed to the lack of significant line emission at 630 nm from the luminous residue at this time.

With the perigee chosen to lie at 53° W magnetic longitude, coinciding with the longitude of the moving lights, its altitude is found to be 88 km. If the perigee is instead assumed to be a slightly smaller 50° W value, then the altitude at perigee becomes 112 km. Slight changes in the location of the perigee don't significantly change our analysis aside from the perigee altitude.

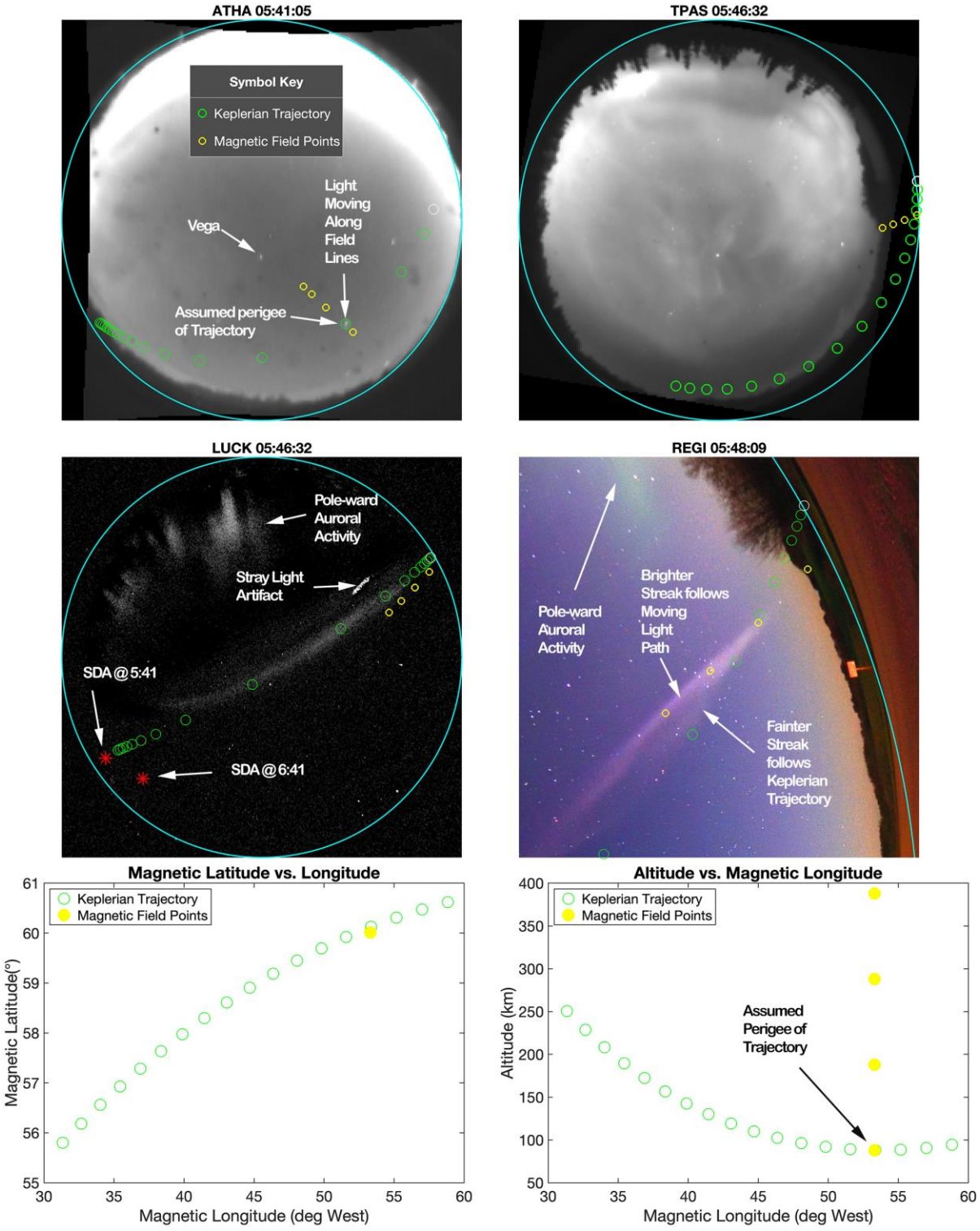


Figure 5. The 3-dimensional structure of the earliest STEVE emission is quantified by parallax analysis.

As soon as STEVE appears in the ATHA imager it is apparent from the movie file showing grayscale ATHA data in the supplemental materials that there are 2 distinct bands of luminosity. The full color (B.J. Jackel, 2014) ATHA keogram spanning the 6:00 to 6:59 time interval displayed in figure 6 confirms the difference in color seen far more clearly in the REGI image between the upper and lower structures. The vertical scale of the keogram is displayed so that it conforms to the vertical extent of the grayscale ATHA image to the left. Here 10 successive frames of LUCK data and 5 frames of the grayscale ATHA data have been co-added to improve the signal to noise ratio for the ASI images. As Vega passes across the center of the ATHA imager it produces the rainbow-colored streak artifact seen near 6:45 in the keogram. In the keogram spanning the 6:00 to 6:59 time interval, it is seen that the lower band has a greenish tinge, while the upper band has a purple hue. In the REGI image at 6:02:48, 3 distinct "green picket fence posts" are indicated. Magnetic field lines corresponding to the location of these 3 posts are shown by the series of yellow circles. For some posts, such as the western-most exemplar case shown in the figure, there is continuity between the green tip and a higher-altitude purple streak. For other posts, there is either a gap between the green tip and higher-altitude purple streaks, or no corresponding co-linear purple streak visible. For some cases there are field aligned purple streaks but no collinear green streak. Examples of all of these possibilities can be seen in the 6:02:48 REGI image.

In the REGI movies in the supplemental materials, a much larger number of green picket fence post examples can be seen. The motion of each of the Objects -1 through -6 can be seen in these movies, together with additional transient streaks labeled with letters. The numerous transient events not detectable in the other ASI data sets because of their lower sensitivity are most likely satellites, but without a confirmation of altitude this cannot easily be confirmed. Several frames in the REGI movies exhibit a transient diffuse green glow that is occasionally observed. A few transient events are observed to blink regularly and are identified as aircraft with flashing collision avoidance lights. A few single frame streaks are identified as conventional meteors based on their appearance.

A straight line running approximately through the lower altitude extreme of the picket fence posts in figure 6 is indicated by the 7 orange pentagrams evenly spaced along the line. This straight line runs through the lower band labeled "Green Picket Fence" in the ATHA image and keogram. The green structures are not visible in the LUCK imager as they have little intensity in the narrow 630 nm band. The "Narrow Purple Band" indicated by the points along the "Keplerian Trajectory" is at a distinctly higher altitude than when it first appeared, although its magnetic coordinates have not changed significantly, as can be seen in figure 3. The location of the "Narrow Purple Band" at the latest time 6:34 that it is seen significantly in both LUCK and ATHA has not significantly further changed in altitude but has apparently drifted a bit southward or possibly westward.

As best seen in the ATHA movie from the supplemental materials, blobs of relatively brighter luminosity in the upper and lower bands are observed to move in a coordinated fashion, so that a typical upper and lower blob in an associated pair lie along a common magnetic field line. These field lines appear approximately as "radial bicycle spokes" (such as the field lines indicated in figure 6 by the yellow circles) that are moving about the center of the ATHA image movie. Although it is somewhat difficult to be precise, considering the "fuzziness" of the blobs, it was found that the *apparent* velocity for blobs in the upper band was initially directed downwards along the band at a speed of several km/s. In contrast, the *apparent* velocity for blobs

in the lower band was directed horizontally along the band at a speed of somewhat less than the speed in the upper band. These speeds are comparable to the westerly ion speed seen by SWARM (E. A. MacDonald, 2018). It seems highly unlikely that there are actual physical blobs of luminous material descending at such a rapid speed along the upper inclined STEVE band. It is also highly implausible for there to be a population of lower altitude blobs that just happen to move at a speed such that they remain on the same magnetic field lines as their higher altitude partners! The resolution of this apparently paradoxical appearance is explained below.

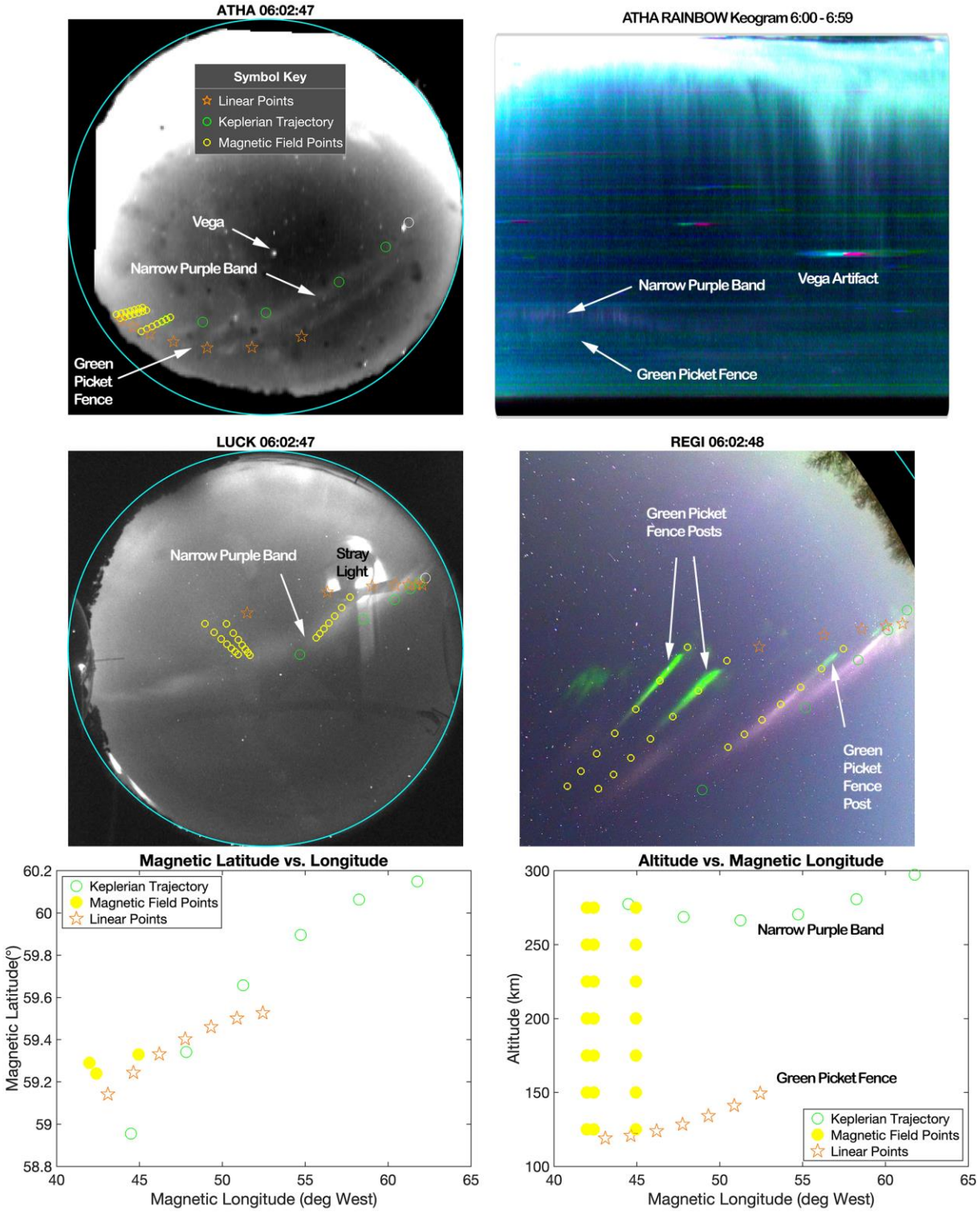


Figure 6. The 3-dimensional structure of the Green Picket Fence is quantified by parallax analysis.

### 3.8 STEVE Pulsations

It is found that the intensity of the STEVE emission is, in certain places, pulsating with a period of about 1 minute, as shown in figure 7. In this figure, the integral intensity within the

Region of Interest (ROI) shown in blue for the signal is corrected by the subtraction of the average background per pixel determined in the red ROI. A similar procedure is used for an estimation of the intensity within the electron aurora appearing to the north of STEVE, except that the Aurora result plotted has a linear background subtracted for each color and also an arbitrary linear scaling applied for convenience of display in the plot.

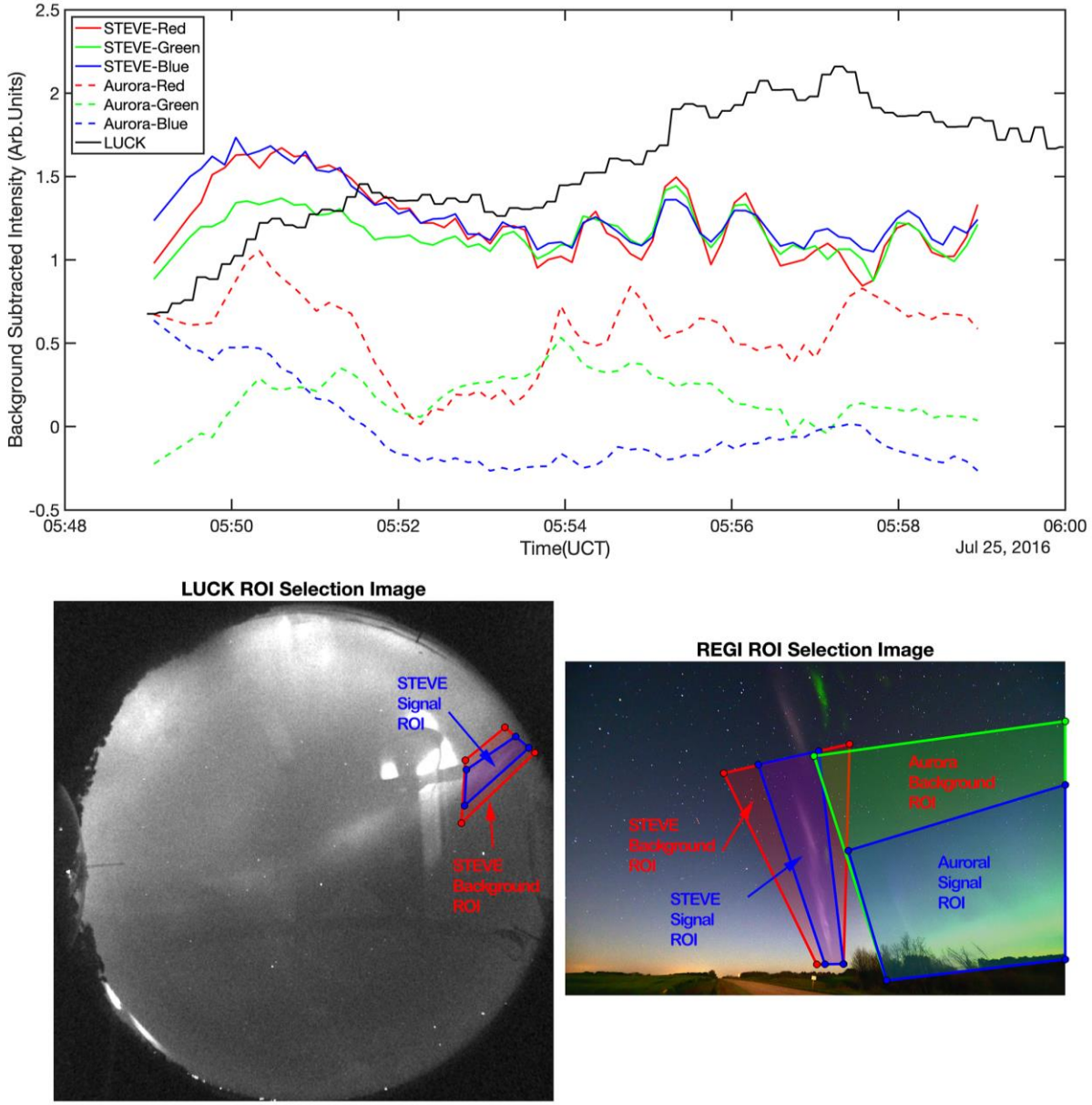


Figure 7. Pulsations in the luminosity of STEVE emission in the indicated ROIs is plotted in the upper graph. The lower images show the boundaries of the ROIs used.

Weaker pulsations at this same period are observed in the 630 nm LUCK data. The STEVE pulsations are apparent in the playback of the supplemental movie in the (E. A. MacDonald, 2018) reference. It can also be noticed that the pulsations in STEVE are correlated with the much weaker pulsations in the electron aurora seen to the north. The pulsations in

STEVE appear to be approximately 180° out of phase with respect to the electron auroral pulsations.

The period of STEVE pulsations appears to be unusually long compared to the normal range 2-20 s of auroral pulsations (Johnstone, 1978). The period seen here cannot be long because of an aliasing artifact, as it is seen in both REGI data with an 8.4 s sampling interval and LUCK with a 3 s sampling interval. The long period also does not seem to be associated with the larger "off" and shorter "on" times associated with long period pulsating aurora (Yamamoto, 1988), as the intensities appear to be nearly sinusoidal while fluctuating.

Although the STEVE pulsation period is unusually long, the fact that it is so highly correlated with the electron auroral pulsations indicates that the narrow purple band structure of STEVE is energized by auroral activity and is not solely an ionospheric phenomenon.

## 4 Bombardment-induced Light Emission

According to (Thomas, 1979) "An inescapable consequence of the bombardment of a solid with atomic particles in the energy range above a few tens of electron volts is the emission of particles from the solid via sputtering. A fraction of the sputtered flux emerges from the solid surface in an electronically excited state and gives rise to the emission of light in a volume outside the surface". This phenomenon is known as Bombardment-induced Light Emission (BLE). As the energy of auroral particles is well above this threshold, it is to be expected that upon encountering solid bodies, such as those identified as objects-1 through -6, substantial light emission will take place.

Although BLE of solids is a general phenomenon occurring in a wide variety of materials, sputtering by electrons seems to be much more sensitive to the material composition (Townsend, 2005). We will refer to Auroral BLE, whether by electrons or ions and whether by trapped or precipitating particles as ABLES.

ABLES can account for the rapid variations in the observed light intensity shown in figure 3, especially object-1. With the assumption that the object is tumbling as it passes through the region of auroral bombardment, and that as different materials are exposed to the auroral bombardment, the nature of the emitted spectrum and its intensity will change accordingly.

The spectrum of the emitted light will depend on the nature and energy of the bombarding particles, as well as on the material composition of the solid body. It appears, for example, that the composition of object-2 was more readily illuminated by the electron flux than the proton flux, based on its much lower observed brightness for the lower latitude points. It is suggestive that portions of the object-1 streak in figure 3 resemble the color of STEVE seen at the same time and in the same photograph.

## 5 STEVE hypothesis and answers to questions

Our hypothesis is that STEVE emission in general could be produced by ABLES of solid material, i.e. dust, left behind by the passage of a meteor at some time prior to the first appearance of STEVE. The remnant debris would initially lie along the trajectory of the meteor. From the estimate of the 7-25 meteor's trajectory, it would have passed almost directly over the REGI location. Even though there is no photographic evidence to confirm or deny the existence of this meteor at the time of its passage, N. Bourassa would have certainly noticed a *normal* meteor passing across the entire sky but did not, and no such visible meteor trail appears in any of his photographs. The ATHA 5:41 flashes would have been only barely above the REGI horizon and would plausibly not have been noticed by N. Bourassa. The perigee of this

hypothetical meteor must have been at sufficiently high altitude that ablative heating did not produce sufficient luminosity for the meteor to be noticed from the ground or detectable in the ASI cameras. On the other hand, the perigee of the hypothetical meteor must have been at sufficiently low altitude to produce an extended trail of dust. The estimated altitude of the perigee described in section 3.6 does indeed lie near the threshold between normally visible and normally invisible meteors (Plane, 2012).

In the absence of bombardment by auroral particles, this debris would remain nearly invisible, as is found to be the case for all 6 objects shown in figure 3 over the portions of their trajectories significantly poleward of the auroral region of bombardment. Just as a laser beam in air may only become visible upon passage through a region of smoke or dust, STEVE emission could become visible only where both remnant dust and auroral bombardment coexist. The narrow width of STEVE emission relative to SAID events is explained by the narrow width of the dust distribution. The green picket fence features could also be produced by secondary electrons from the sputtering of remnant material that continue to travel down along field lines, producing typical auroral emissions in collisions with the lower atmosphere. That secondary electrons would be constrained by the local field lines explains the co-location of the green picket fence with the higher altitude narrow purple bands in STEVE in magnetic coordinates. It appears that a population of sputtered ions (not necessarily as tightly constrained as the sputtered electrons to magnetic field lines because of multiple charge exchange collisions) could perhaps be responsible for the very diffuse glow most clearly seen in the last frame of one of the REGI movie in the supplemental materials. In the event of insufficient sputtered intensity, the picket fence would not be detectable. The picket fence is at nearly constant altitude as it is produced in typical auroral fashion by the secondary ions and electrons exciting atmospheric gaseous components. The exponential increase with depth into the atmosphere produces a relatively sharp altitude definition for the lower end of the picket fence posts. The narrow purple band inclination, in contrast, initially follows the path of the remnant meteor material and need not be horizontal.

In addition to sputtered secondary ions and electrons that travel down along field lines, another population of upward travelling sputtered particles would travel up along field lines, eventually reaching the opposite hemisphere and producing an array of green picket fence structures of comparable intensity to those seen in the northern hemisphere. In the event that the auroral bombardment ions or electrons have a range greater than the typical size of the remnant dust particles, then the downward flux of secondaries would tend to be greater than the upward flux. On the other hand, for remnant dust particles larger than the range of the bombarding auroral ions, the upward flux would tend to be dominant, as more “backsplash” sputtering would occur. The “strikingly different” upward FAC seen in the STEVE event (Y. Nishimura, 2019) with a conjugate structure in the opposite hemisphere could be associated with the flux of such sputtered secondary “backsplash”. It is possible that the moving lights seen in the ATHA images near 5:41 could be associated with such “backsplash” occurring in a momentarily intense protonic bombardment event acting on the meteor at that time.

Among the 1408 ATHA images taken between 5:39 and 7:59 there are a total of 9 isolated “flash” events similar to the 5:41 event, but none of them last as long or are as intense. It seems possible that these other isolated flashes are also “backsplash” from sputtering of meteors or sub-visual satellites, but without simultaneous observations of these isolated flashes in other imagers, this is only speculation. It can be seen in the movies included in the supplemental materials that there are very frequent isolated, single frame “flash” events in the LUCK images,

but we have not been able to find simultaneous observations of corresponding flashes in any of the other imagers in this case either.

Although there are no reports of southern hemisphere streaks for the 2016-7-25 event, it is shown in (Y. Nishimura, 2019) that conjugate streaks are seen in a STEVE event with green picket fence structure, but not in the case of an event without the green picket fence. If the narrow purple streaks seen in STEVE are all produced by ABLES of dust, then they would only be seen in one hemisphere, while secondary sputtered particles of sufficient energy and intensity to produce the green picket fence could produce green picket fence structures seen in both hemispheres.

That STEVE events seem to share a common purple hue in photographs can be attributed to the homogeneity of the materials in the dust left in the remnant trails of ionospheric meteors together with the primarily protonic ABLES of these materials.

The apparent motion of blobs of luminosity seems to be at a speed of several km/s along the longitudinal extent of STEVE. Rather than an actual motion of the STEVE material, in the present picture, this is an illusory motion that rather corresponds to local peaks of auroral bombarding flux that pass across the remnant dust trail and illuminate different regions of the dust as a function of time. This is just as laser beam directed to different regions of a smoke cloud would appear to produce a moving spot of light, but the motion of this light would not reflect the motion of the smoke particles.

## 6 Novel observations via ABLES

ABLES of satellites and meteors provides a good explanation for the variations of their emissions as they pass through regions of concurrent auroral activity. Assuming this explanation is correct, then a much larger number of such events could be detected by correlating images from pairs of cameras as sensitive as the REGI camera by simultaneously observing similar patches of sky during auroral activity from appropriately sited locations. In July 2016, the number of known satellites cataloged in (Kelso, 2019) was 19,751. The number having a perigee less than 2,000 km was 16,506. Among these LEO objects, 14,111 had an orbital inclination angle of 90°±30°. On the average, in the 18-minute period during which 31 transient streaks were observed in REGI, approximately 70 of these satellites would have crossed the REGI field of view. It seems that the REGI camera sensitivity was sufficient to detect a substantial fraction of the known satellites that crossed through its field of view.

Although the ASI cameras had the virtue of wide spatial coverage, their limited sensitivity greatly reduced the number of events that could be unambiguously identified as high-altitude objects. Future observations of this phenomenon could open a new window for exploration of the ionosphere during periods of auroral activity. The RGB color vignettes shown for the 6 objects in figure 3 illustrates some of the possible additional characterization that could be extracted for these solid bodies.

**Acknowledgments, Samples, and Data**

- The authors declare no competing interests.
- The data supporting the conclusions of this work can be readily obtained from the cited references together with the files in the supplemental information
- The 16-bit registered REGI photographs used in this work are available from https://doi.org/10.6084/m9.figshare.c.4658714.v1 (Bennett, 2019)

# References


A. Le Pichon, J. G. (2002). Trail in the atmosphere of the 29 December 2000 meteor as recorded in Tahiti: Characteristics and trajectory reconstitution. *Journal of Geophysical Research, 107*(D23), 4709-4718.

A. Olech, P. Z. (2013). PF191012 Myszyniec-highest Orionid meteor ever recorded. *Astronomy & Astrophysics*.

B. Gallardo-Lacourt, J. L. (2018). On the Origin of STEVE: Particle Precipitation or Ionospheric Skyglow? *Geophysical Research Letters*, 1-6.

B. Gallarod-Lacourt, Y. N. (2018). A Statistical Analysis of STEVE. *Journal of Geophysical Research: Space Physics*, 9893-9905.

B.J. Jackel, C. U. (2014). Auroral spectral estimation with wide-band color mosaic CCDs. *Geoscientific Instrumentation Methods and Data Systems, 3*, 71-94.

Bennett, C. (2019, September). *Collection of Images for Journal of Geophysical Research Article "Auroral Illumination of Solid Bodies"*. Retrieved from figshare: https://doi.org/10.6084/m9.figshare.c.4658714.v1

Bettonvil, F. (2005). Imaging Fisheye Lenses. *WGN, Journal of the International Meterior Organization, 33*(1), 9-14.

CIRES. (2019, July). *POMME-10 MAGNETIC MODEL OF THE EARTH*. Retrieved from http://geomag.colorado.edu/pomme-10-magnetic-model-of-the-earth.html

D. Lummerzheim, M. G. (2001). Emission of OI(630 nm) in proton aurora. *Journal of Geophysical Research*, 141-148.

D.M. Gillies, E. D.-L. (2019). First Observations From the TREx Spectrograph: The Optical Spectrum of STEVE and the Picket Fence Phenomena. *Geophysical Research Letters*, 7207-7213.

E. A. MacDonald, E. D.-L. (2018). New science in plain sight: Citizen scientists lead to the discovery of optical structure in the upper atmosphere. *Science Advances*, 1-5.

E. Mishin, Y. N. (2017). SAPS/SAID revisited: A causal relation to the substorm current wedge. *Journal of Geophysical Research: Space Physics*, 8516-8535.

G. Liu, S. E. (2013). Comparison of drift velocities of nighttime equatorial plasma depletions with ambient plasma drifts and thermospheric neutral winds. *Journal of Geophysical Research: Space Physics*, 7360-7368.

Hoffleit, D. a. (2014, January). *Yale Bright Star Catalog*. Retrieved from http://tdc-www.harvard.edu/catalogs/bsc5.html

Johnstone, A. (1978). Pulsating aurora. *Nature, 274*, 119-126.

Jun Liang, E. D. (2016). On the 630 nm red-line pulsating aurora: Red-line Emission Geospace Observaotry observations and model simulations. *Journal of Geophysical Research: Space Physics, 121*, 7988-8012.

K.A. Hill, L. R. (2004). Sputtering and High Altitude Meteors. *Earth, Moon, and Planets, 95*, 403-412.

Kelso, T. (2019, 8). *CelesTrak Home Page*. Retrieved from CelesTrak: https://celestrak.com

Levin, B. Y. (1963). Fragmentation of Meteoric Bodies. *Soviet Astronomy*, 233-238.

Mathworks. (2019, July). *Mathworks*. Retrieved from mathworks.com

P. Lognonne, e. a. (2006). Seismic waves in the ionosphere. *Europhysics news, 37*(4), 11-14.

Plane, J. M. (2012). Cosmic dust in the earth's atmosphere. *Chemical Society Review, 41*, 6507-6518.

S.B. Mende, M. T. (2019). Color Ratios of Subauroral (STEVE) Arcs. *Journal of Geophysical Research: Space Physics*.

Solomon, S. C. (2001). Auroral particle transport using Monte Carlo and hybrid methods. *Journa of Geophysical Research, 106*, 107-116.

Thomas, G. (1979). Bombardment-Induced Light Emission. *Surface Science*, 381-416.

Townsend, P. C. (2005). Sputtering by electrons and photons. In e. R. Behrish, *Sputtering by Particle Bombardment II* (Vol. 52, pp. 147-178). Springer-Verlag.

University of Calgary. (2018, 12 9). *UofC Space Physics Data Portal*. Retrieved from https://data-portal.phys.ucalgary.ca

Vinkovic, D. (2007). Thermalization of sputtered particles as the source of diffuse radiation from high altitude meteors. *Advances in Space Research, 39*, 574-582.

W.E. Archer, B. G.-L.-M. (2019). Steve: The Optical Signature of Intense Subauroral Ion Drifts. *Geophysical Research Letters*, 6279-6286.

Weisstein, E. (2109, July 22). *Gnomonic Projection*. Retrieved from http://mathworld.wolfram.com/GnomonicProjection.html

X. Chu, D. M.-L. (2019). Identifying the magnetospheric driver of STEVE. *Geophysical Research Letters*.

Y. Fujiwara, M. U. (1998, February 1). Meteor luminosity at 160 km altitude from TV observations for bright Leonid meteors. *Geophysical Research Letters, 25*(3), 285-288.

699 Y. Nishimura, B. G.-L. (2019). Magnetospheric Signatures of STEVE: Implications for the Magnetospheric Energy
700 Source and Interhemispheric Conjugany. *Geophysical Research Letters*, 5637-5644.
701 Yamamoto, T. (1988, February 1). On the temporal fluctuations of pulsating auroal luminosity. *Journal of*
702 *Geophysical Research, 93*(A2), 897-911.
703

**Figure 1.**

ATHA 05:54:47

Vega

REGI 05:54:48

NORTH

Object 2

Object 1

WEST

Arcturus

SOUTH

**Symbol Key**

- LUCK Gnd Station
- REGI Gnd Station
- ATHA Gnd Station
- TPAS Gnd Station
- Keplerian Trajectory
- Parallax Tracks
- Ad Hoc Points
- Magnetic Field Points

LUCK 05:54:47

Stray Light

Object 2

Arcturus

Vega

Saturn

Mars

REGI 05:54:48

Object 2

Object 1

Arcturus

**Figure 2.**

ATHA 05:54:35

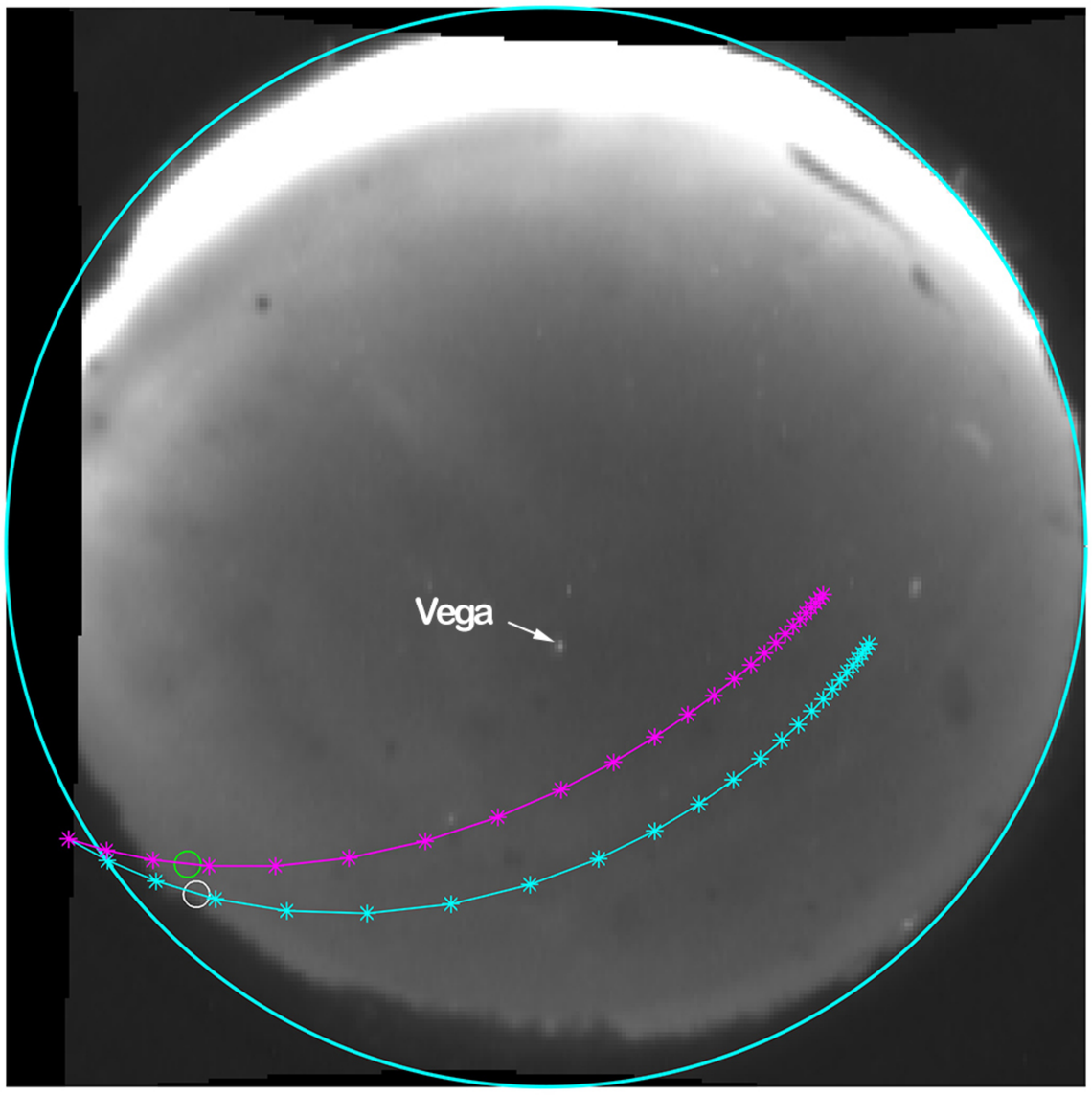


Meteor Brightness vs. Altitude

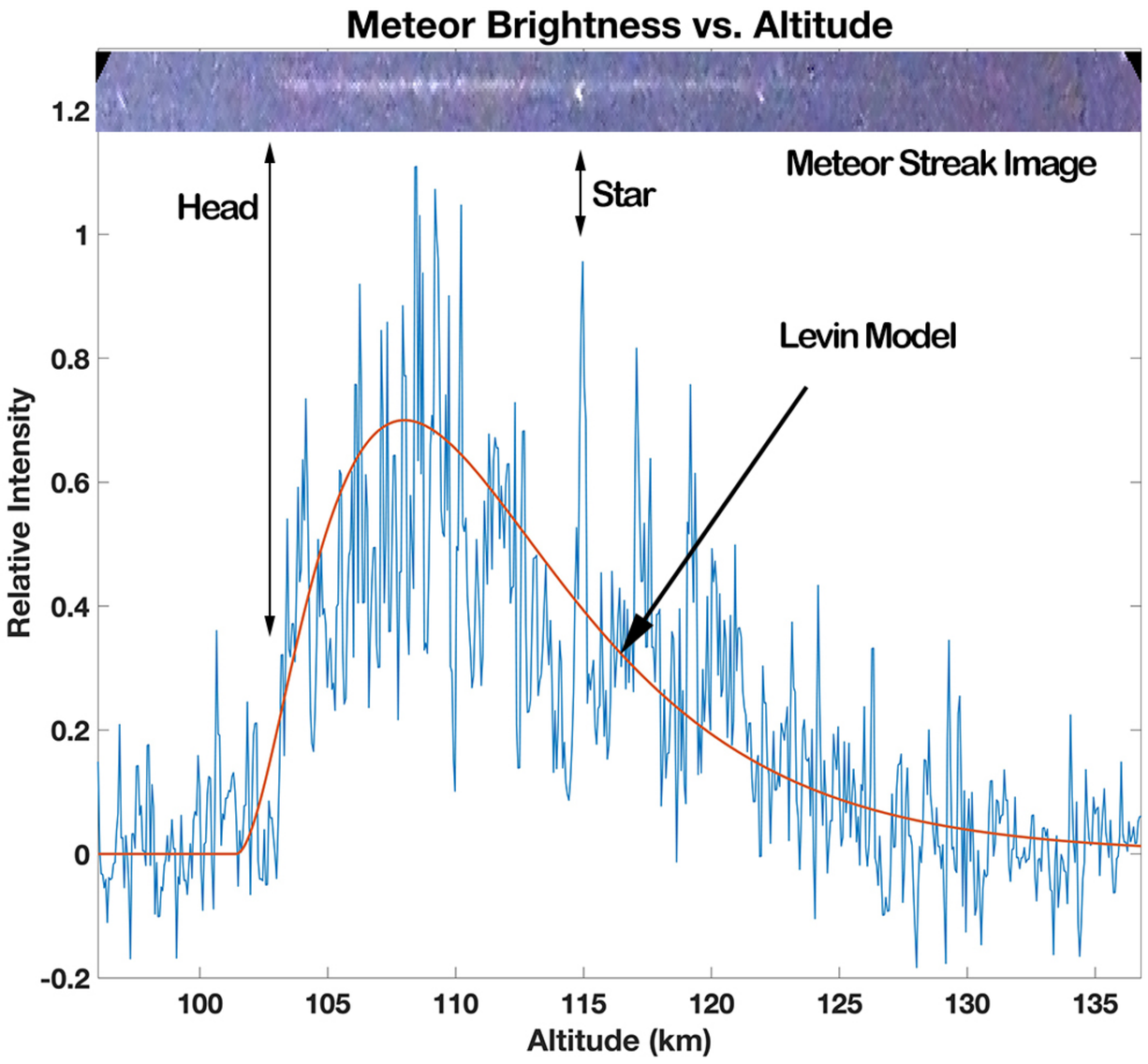


LUCK 05:54:38

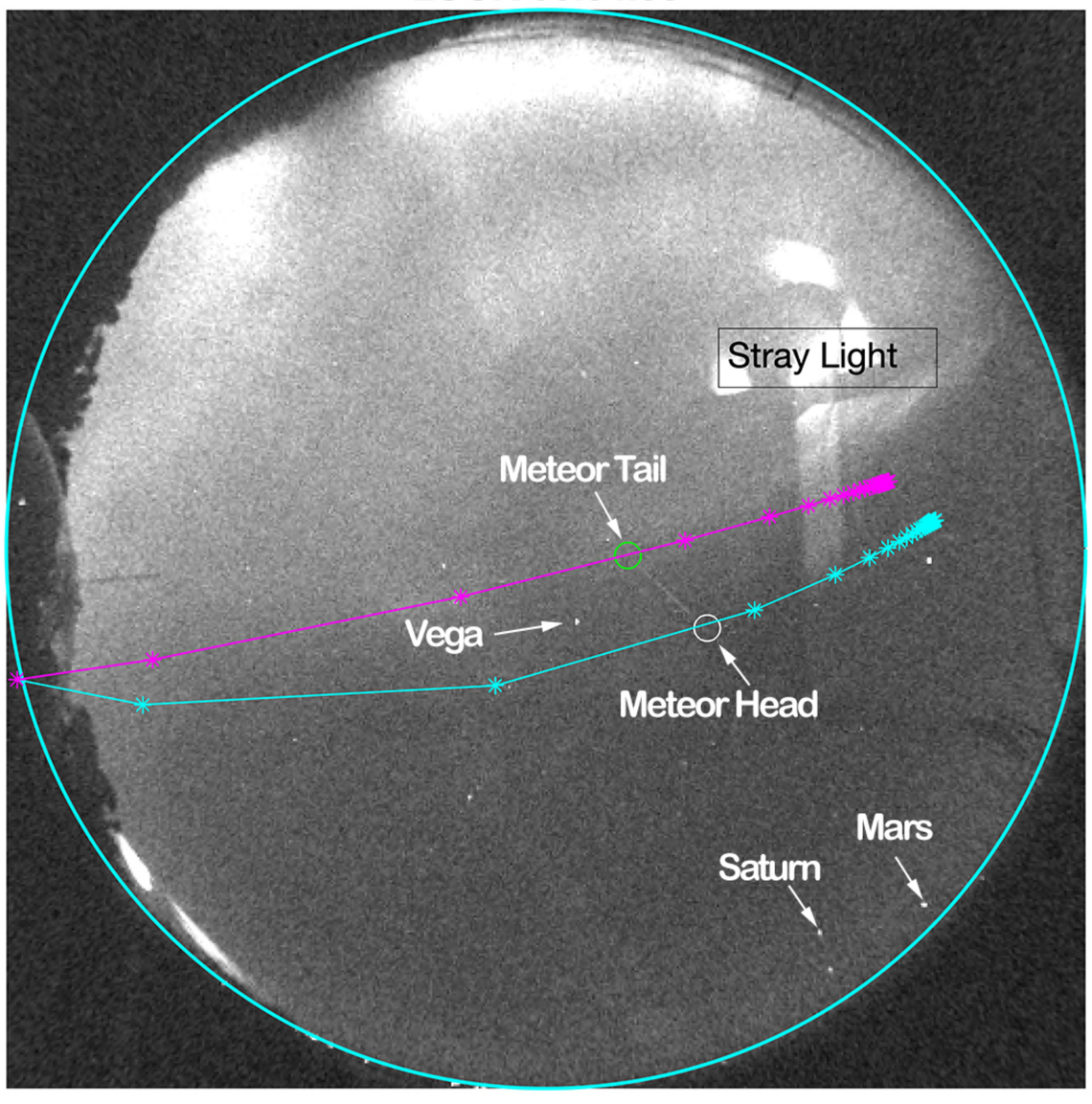


REGI 05:54:39

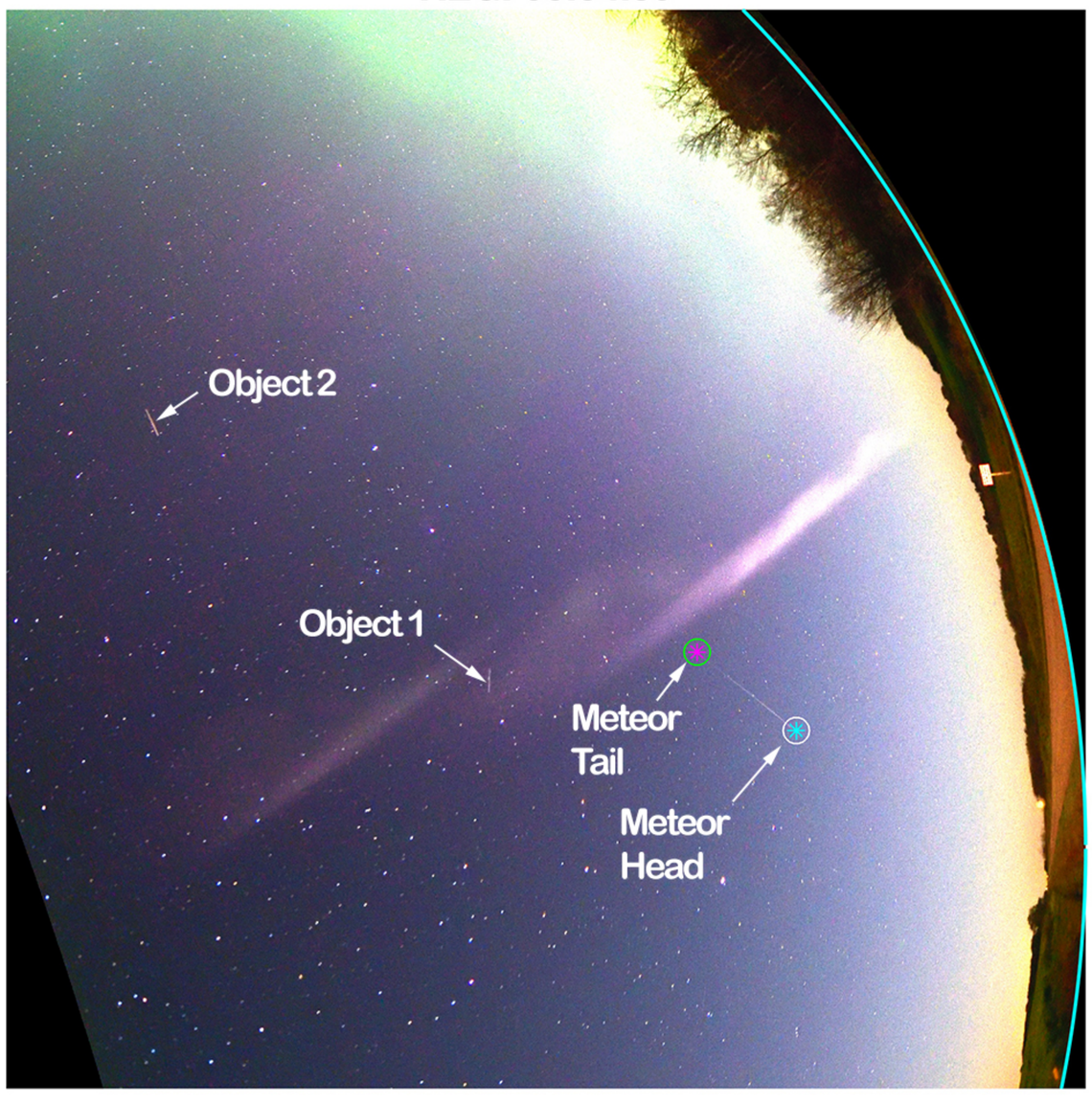

**Figure 3.**

## Object Brightness vs. Time

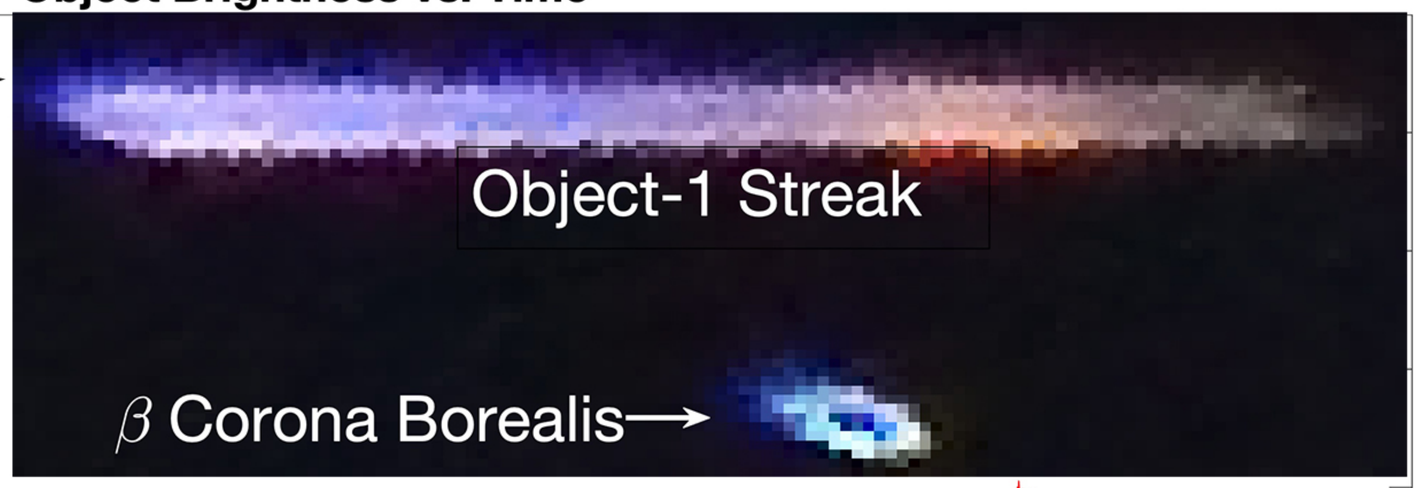


Apparent Magnitude

Object-1

Object-2

Time ( s )

Relative Intensity

Magnetic Latitude (degrees)

ln electron flux

ln proton flux

| Object# | Altitude | Speed $V_{escape}$ | | Time |
|---|---|---|---|---|
| STEVE | 159-239 | | | 5:50 |
| $Object_1$ | ? | ? | ? | 5:54 |
| $Object_2$ | 737 | 9.0 | 10.3 | 5:55 |
| $Object_3$ | 1111 | 8.5 | 10.0 | 5:56 |
| $Object_4$ | 339 | ? | 10.6 | 5:58 |
| STEVE | 266-297 | | | 6:04 |
| $Object_5$ | 908-1186 | 11.9 | 10.1 | 6:07 |
| $Object_6$ | 643 | 9.1 | 10.3 | 6:10 |
| STEVE | 136-275 | | | 6:34 |

Magnetic Latitude (degrees)

Magnetic Longitude (deg West)

**Figure 4.**

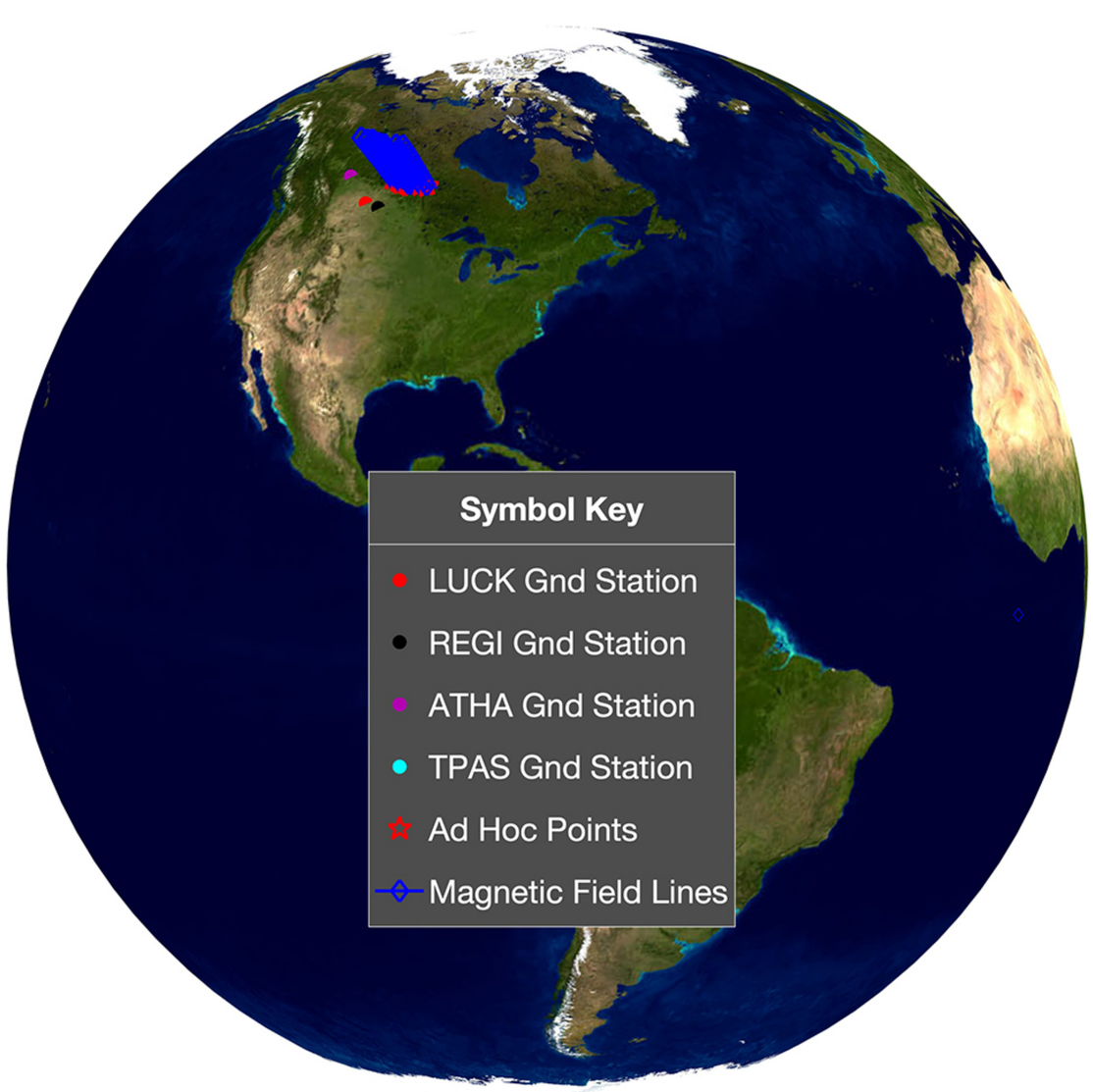
Symbol Key
LUCK Gnd Station
REGI Gnd Station
ATHA Gnd Station
TPAS Gnd Station
Ad Hoc Points
Magnetic Field Lines

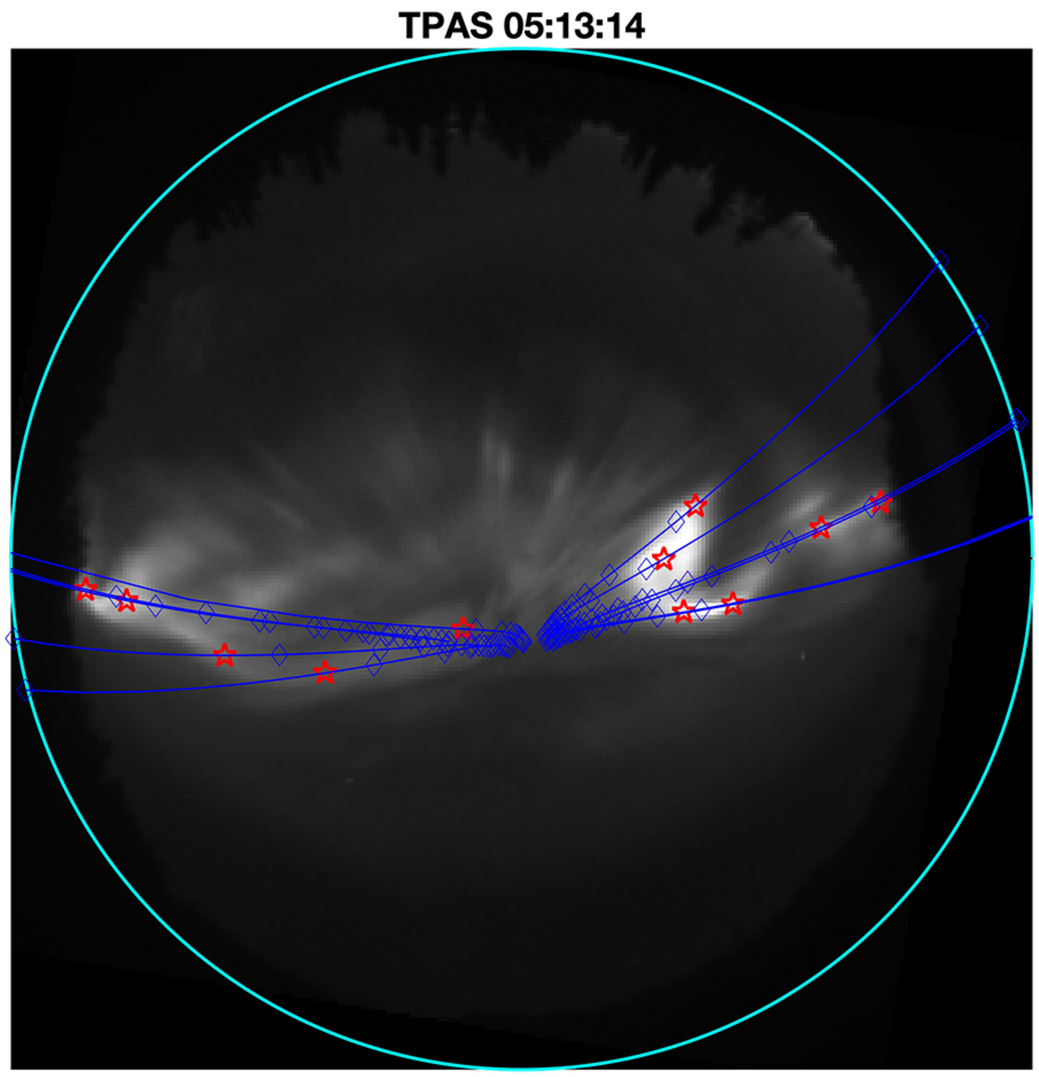
TPAS 05:13:14

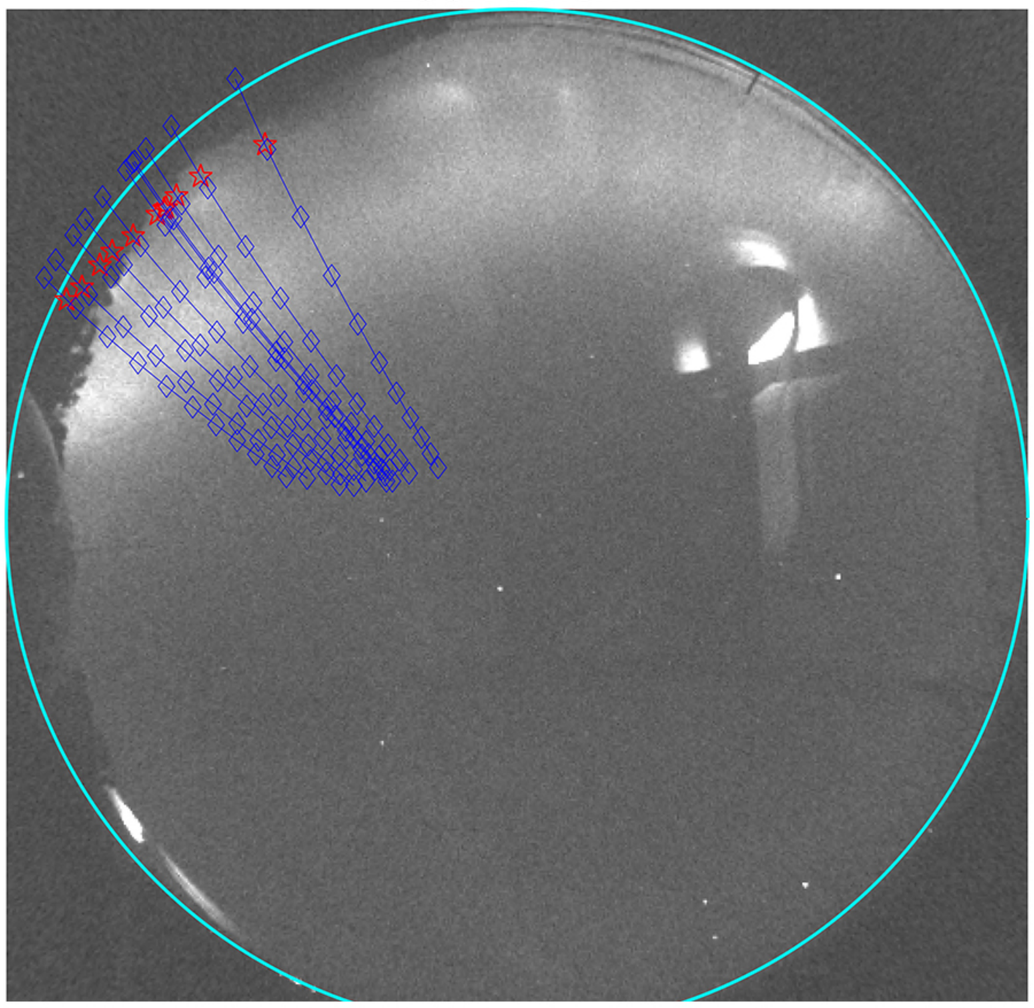
LUCK 05:13:14

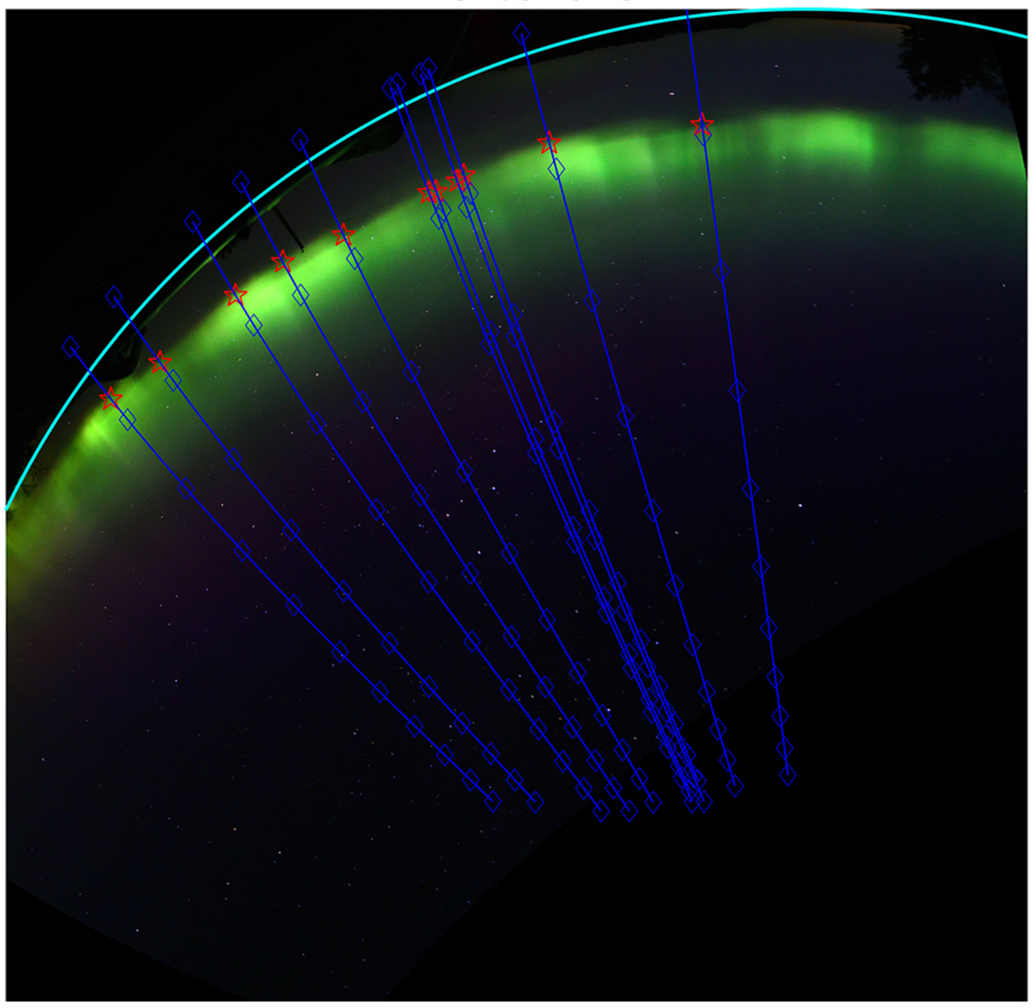
REGI 05:13:18

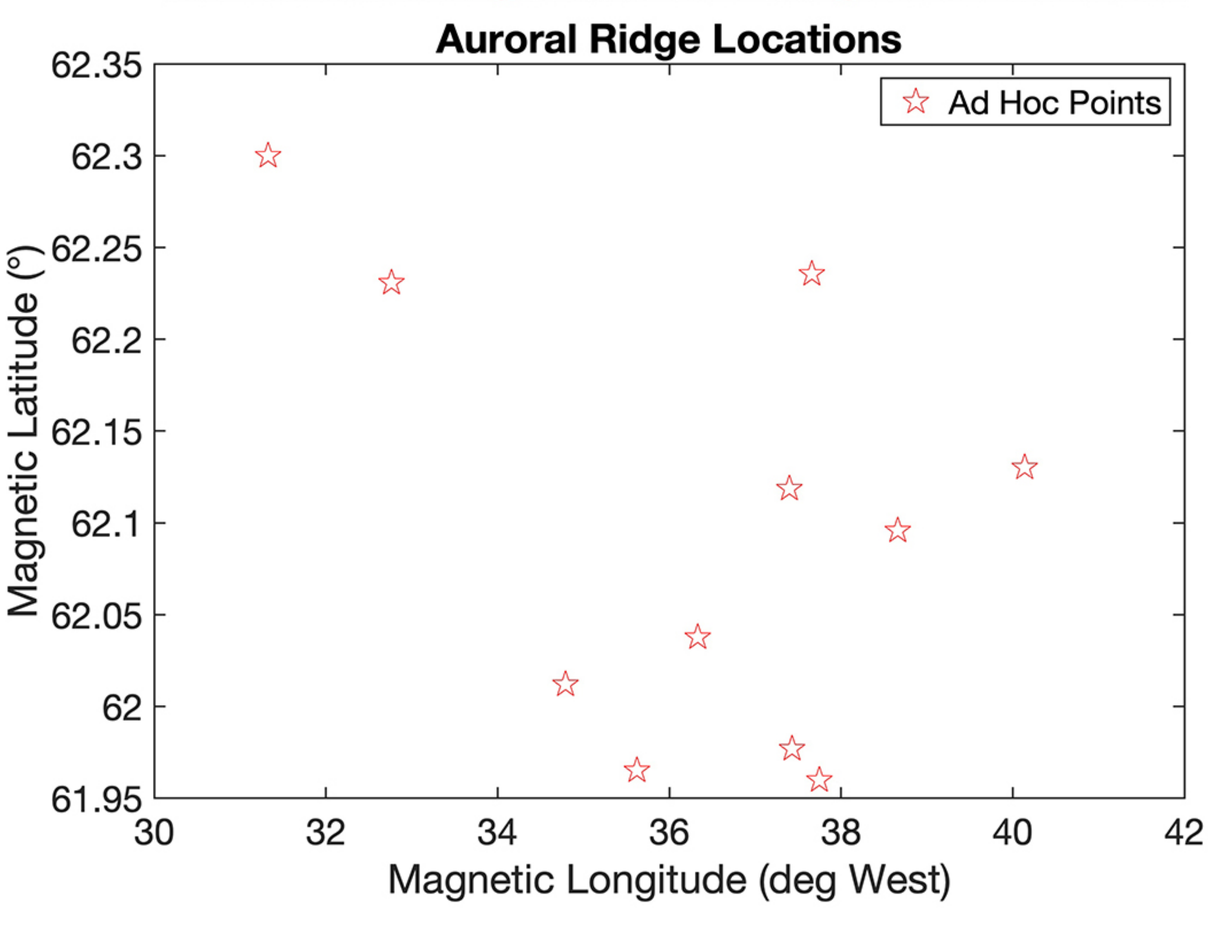
Auroral Ridge Locations
Ad Hoc Points
Magnetic Latitude (°)
62.35
62.3
62.25
62.2
62.15
62.1
62.05
62
61.95
30
32
34
36
38
40
42
Magnetic Longitude (deg West)

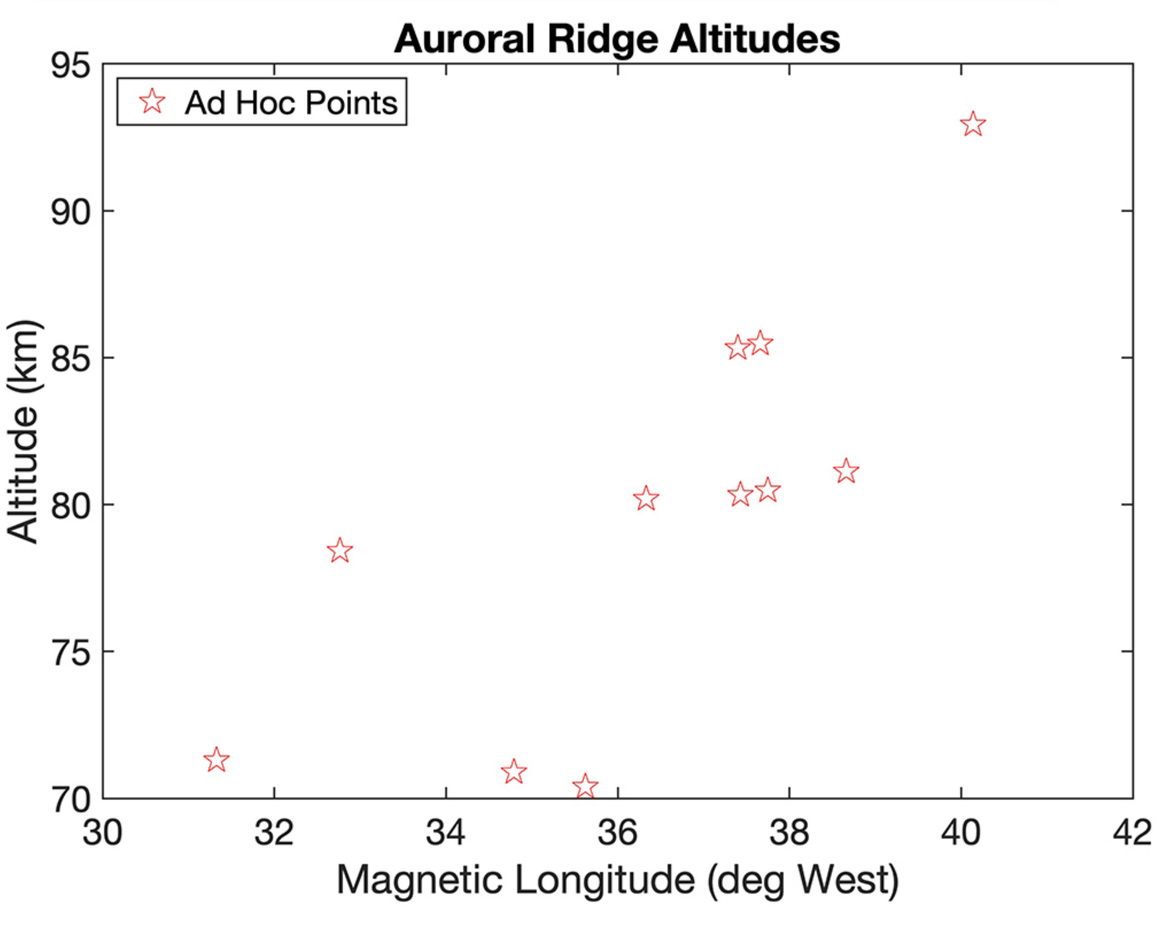
Auroral Ridge Altitudes
Ad Hoc Points
Altitude (km)
95
90
85
80
75
70
30
32
34
36
38
40
42
Magnetic Longitude (deg West)

**Figure 5.**

ATHA 05:41:05

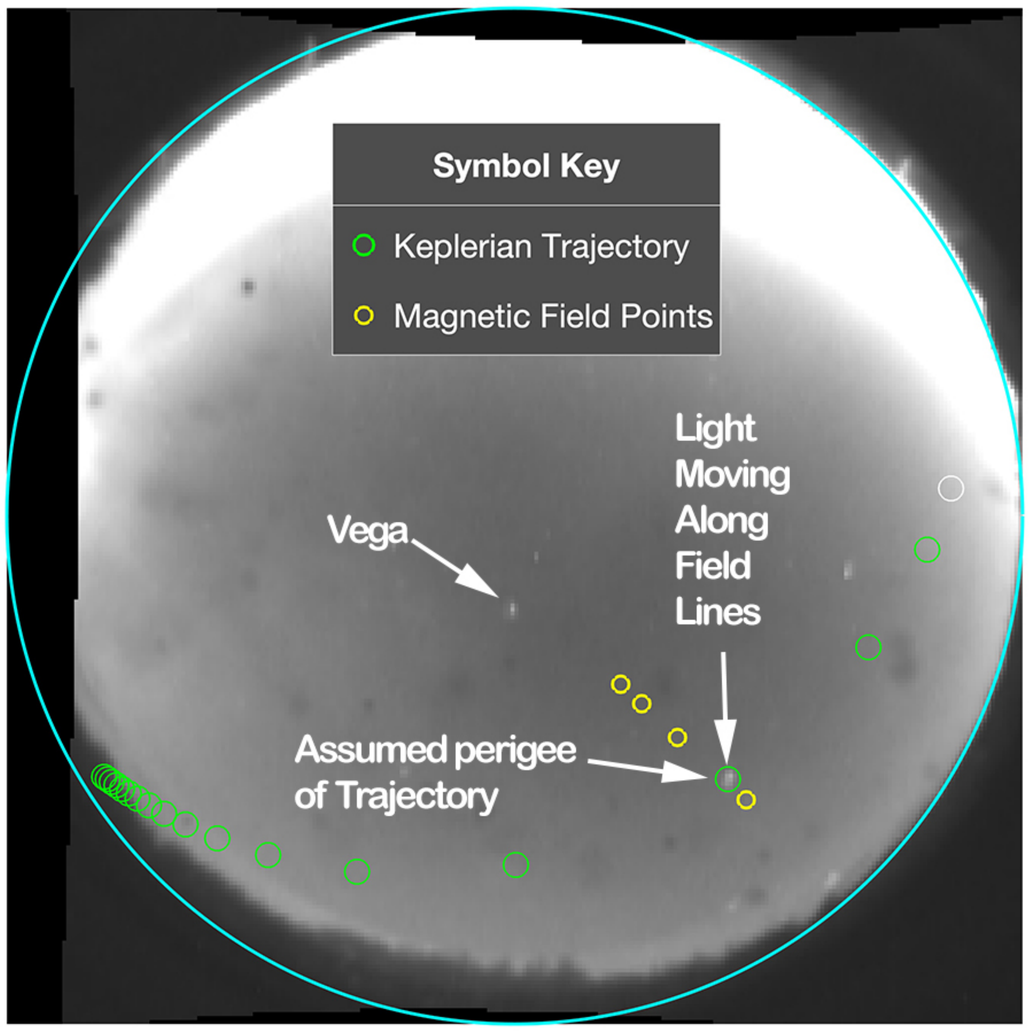


TPAS 05:46:32

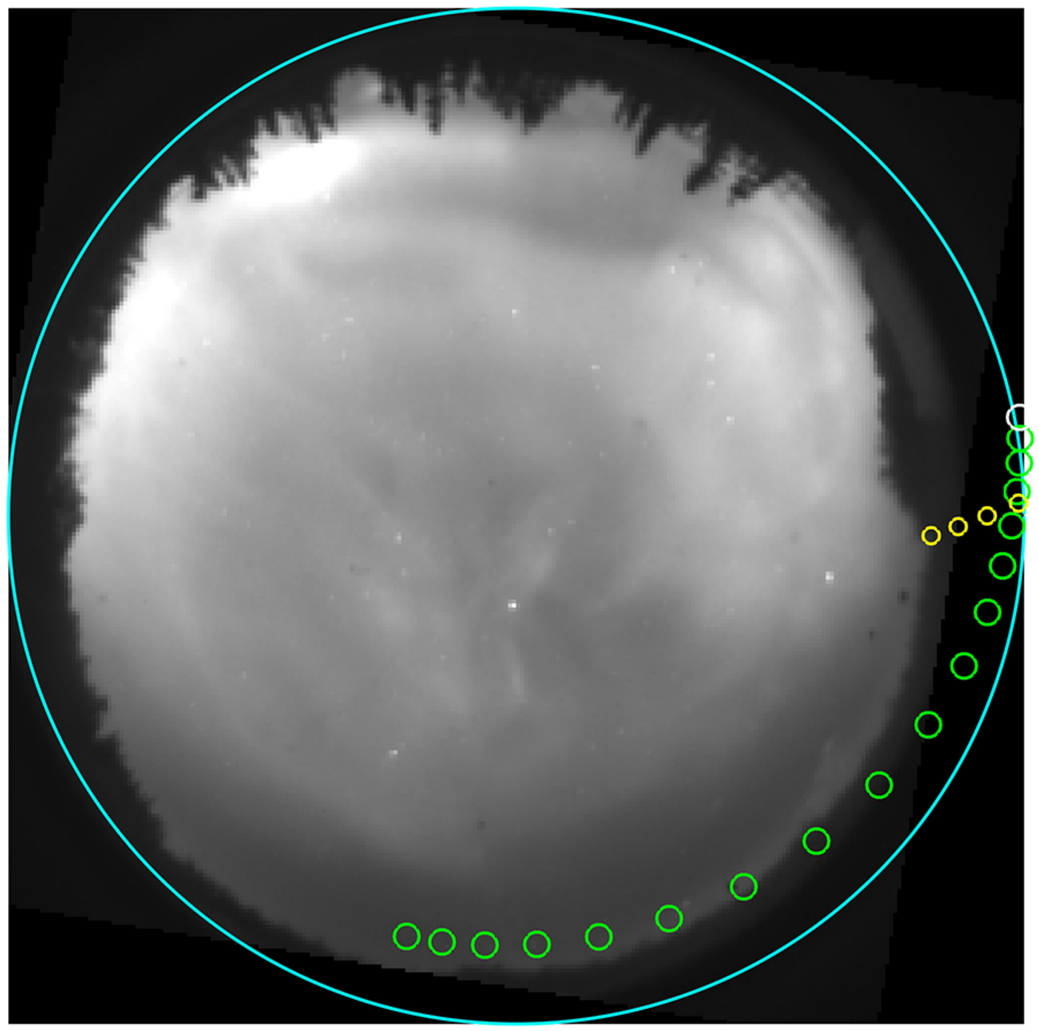

LUCK 05:46:32

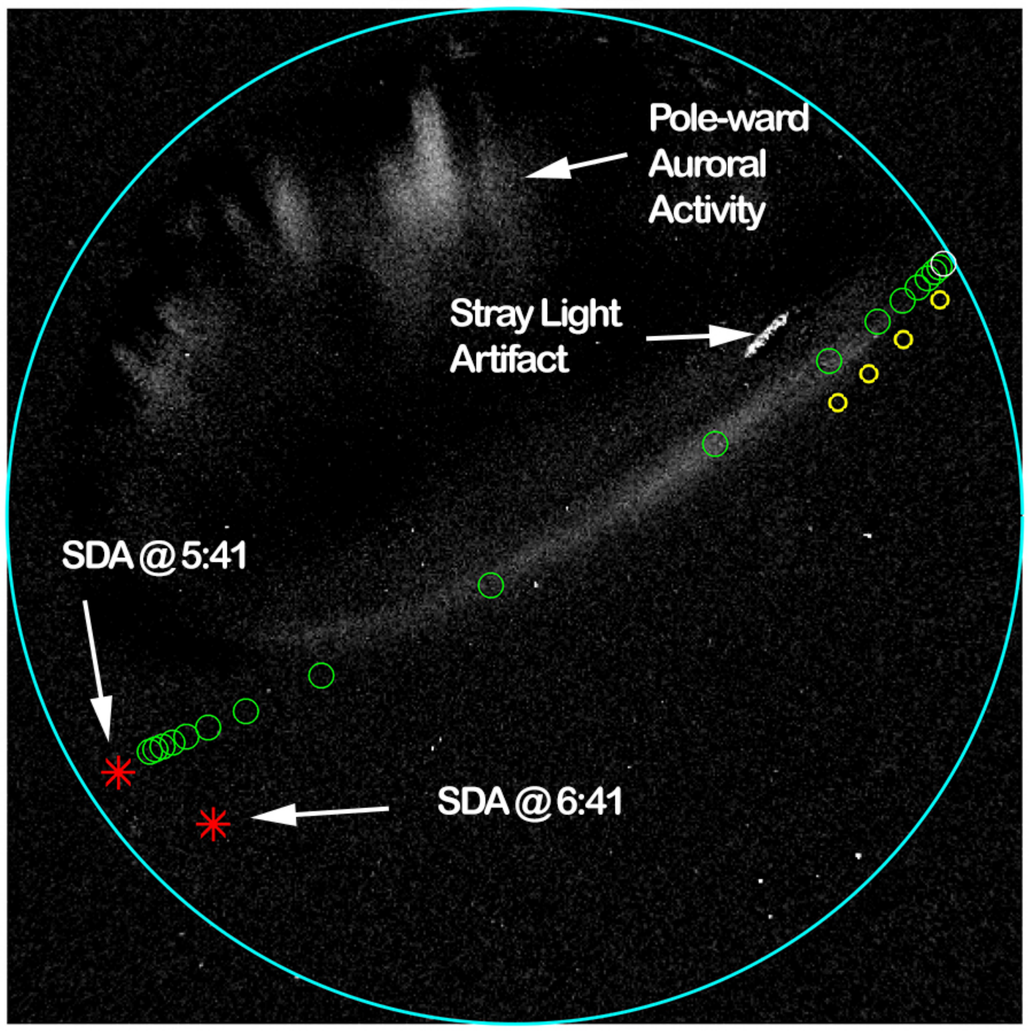


REGI 05:48:09

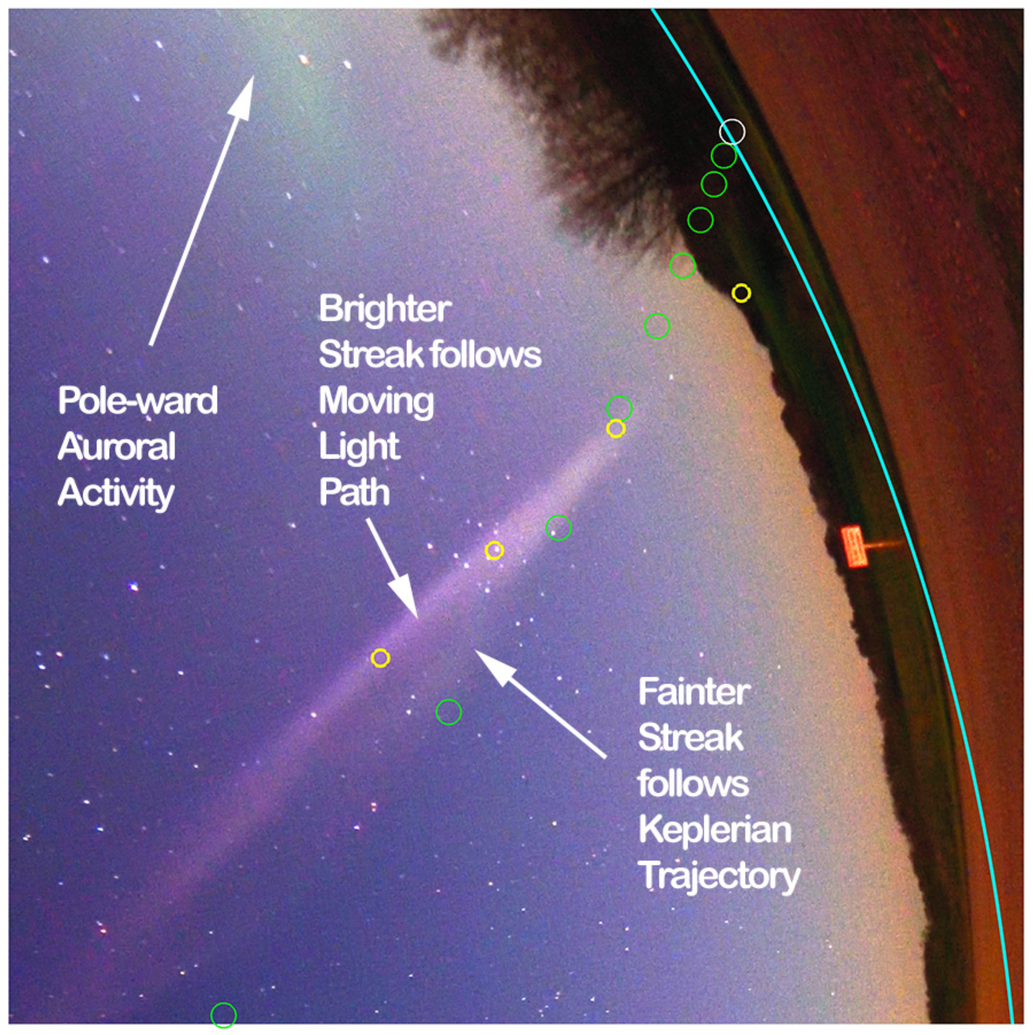


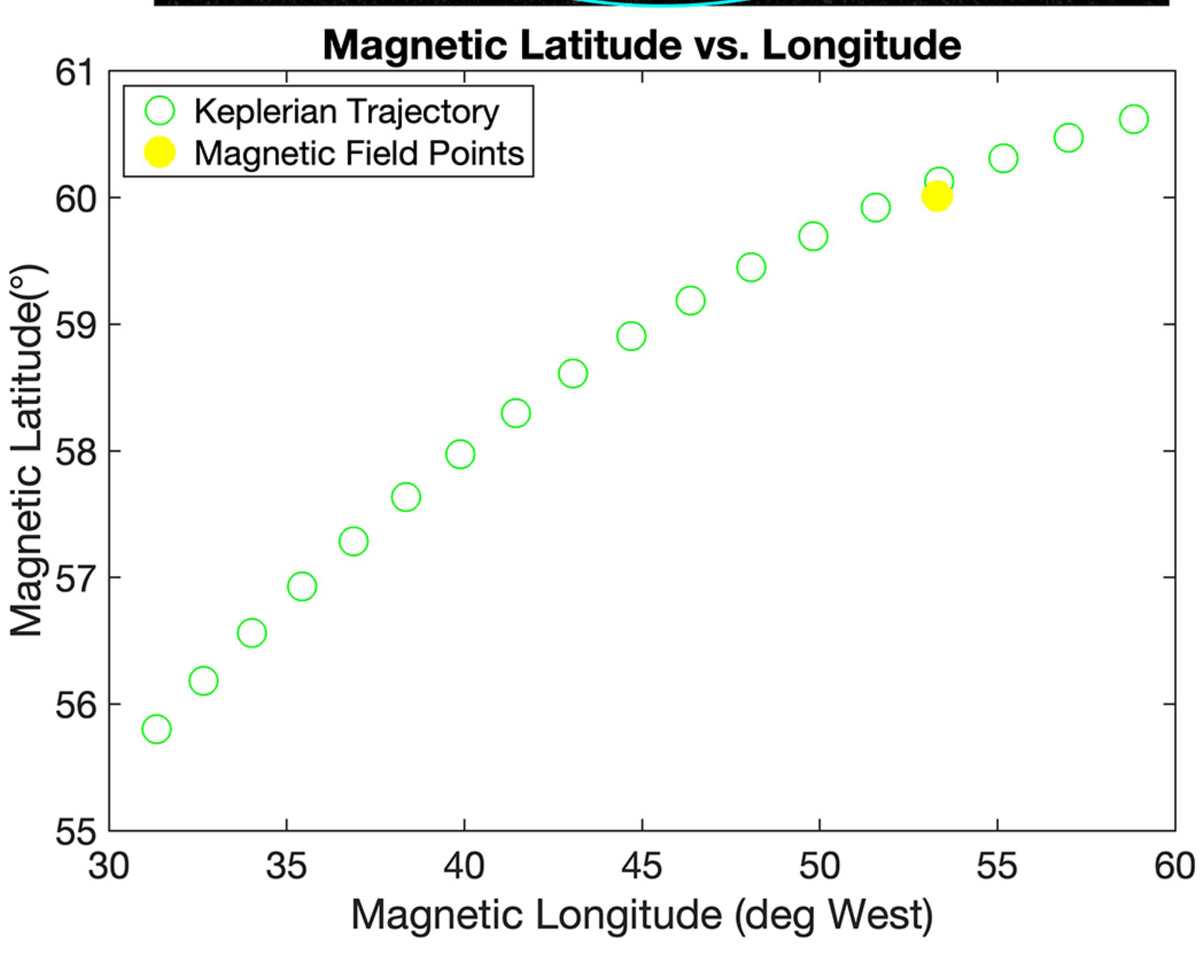


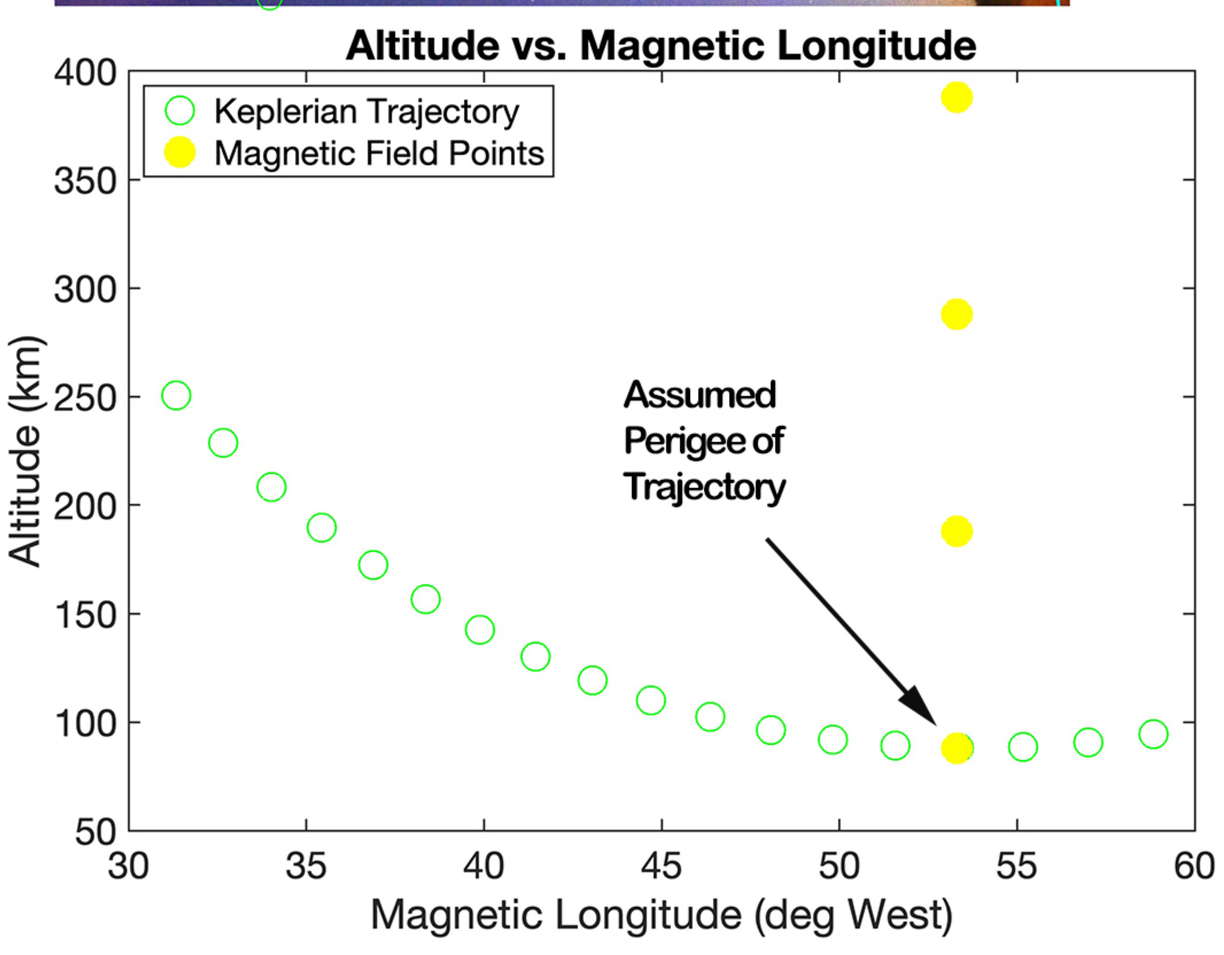

**Figure 6.**

ATHA 06:02:47

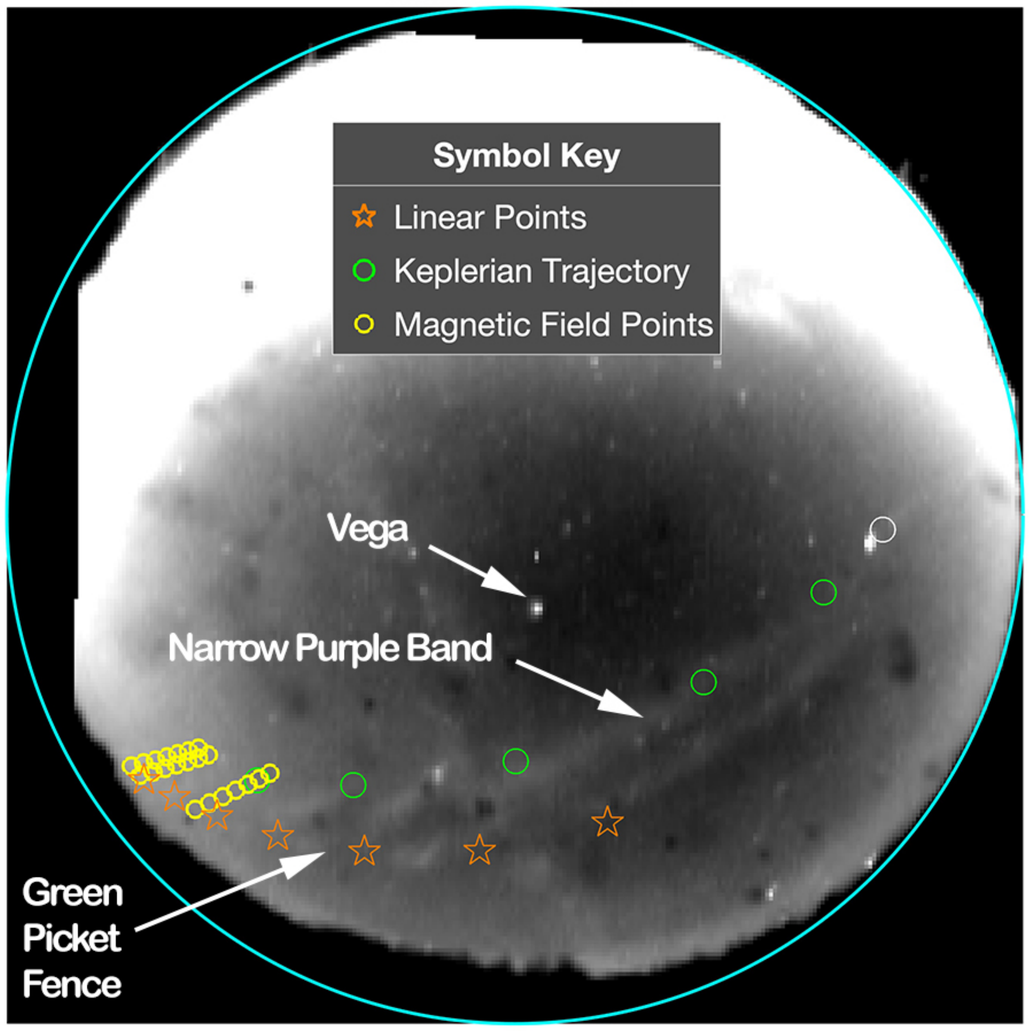


ATHA RAINBOW Keogram 6:00 - 6:59

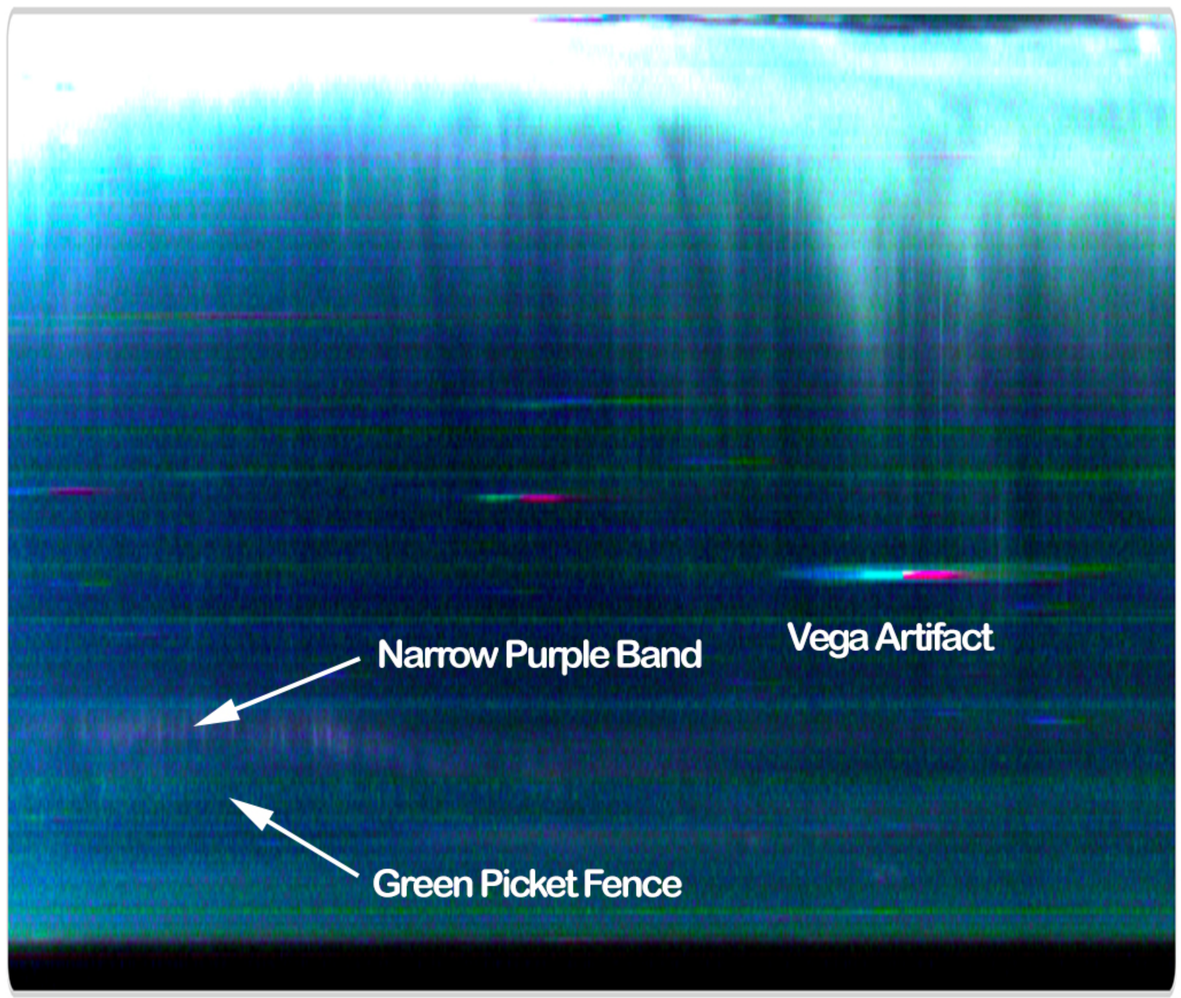


LUCK 06:02:47

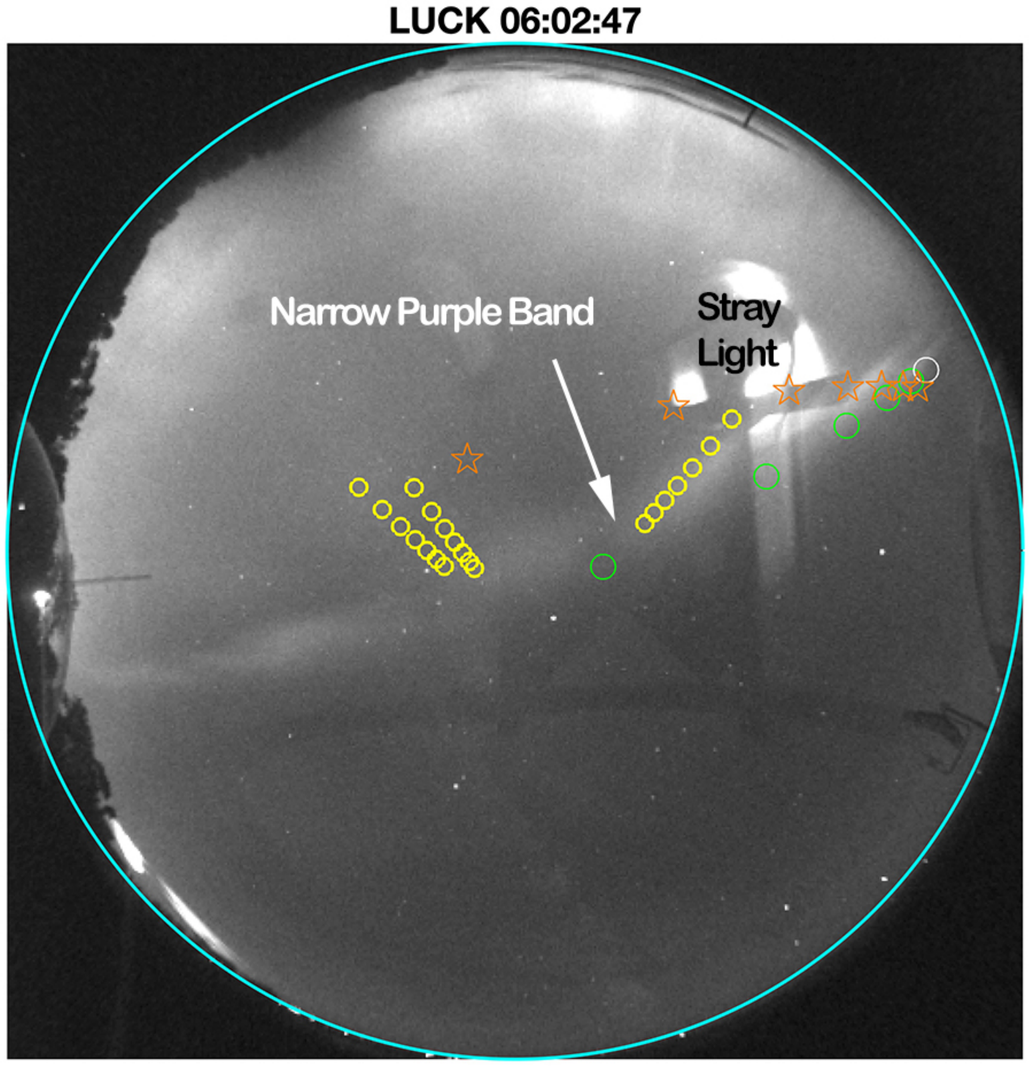


REGI 06:02:48

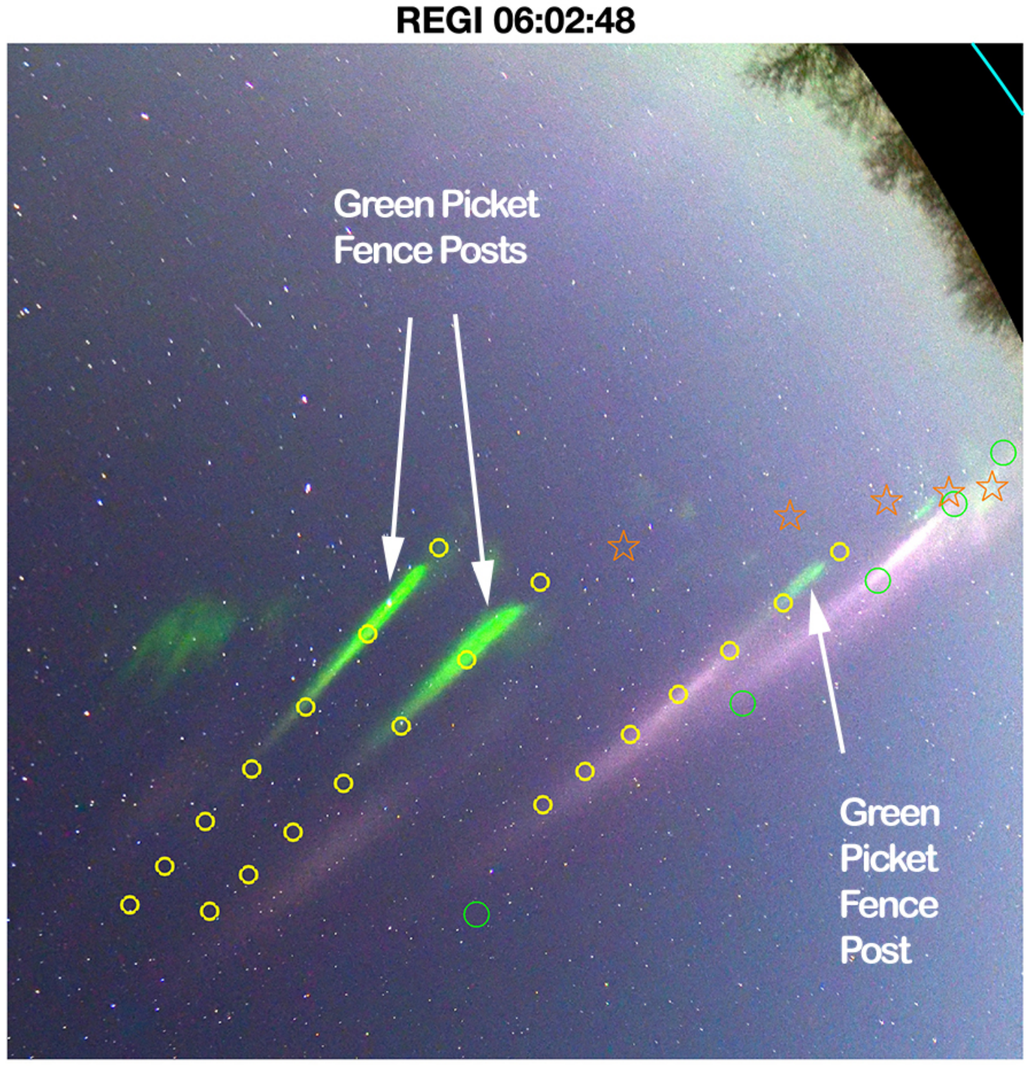


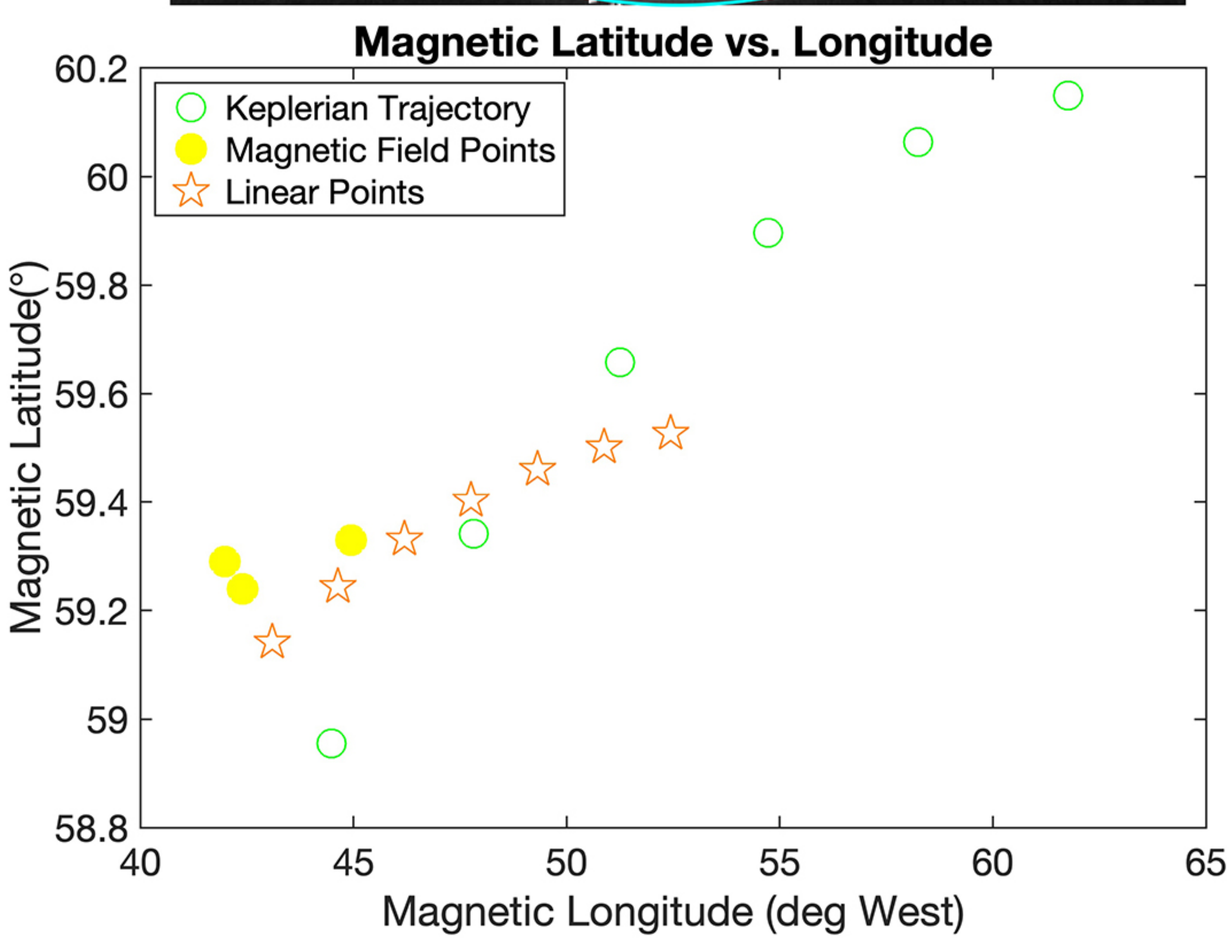


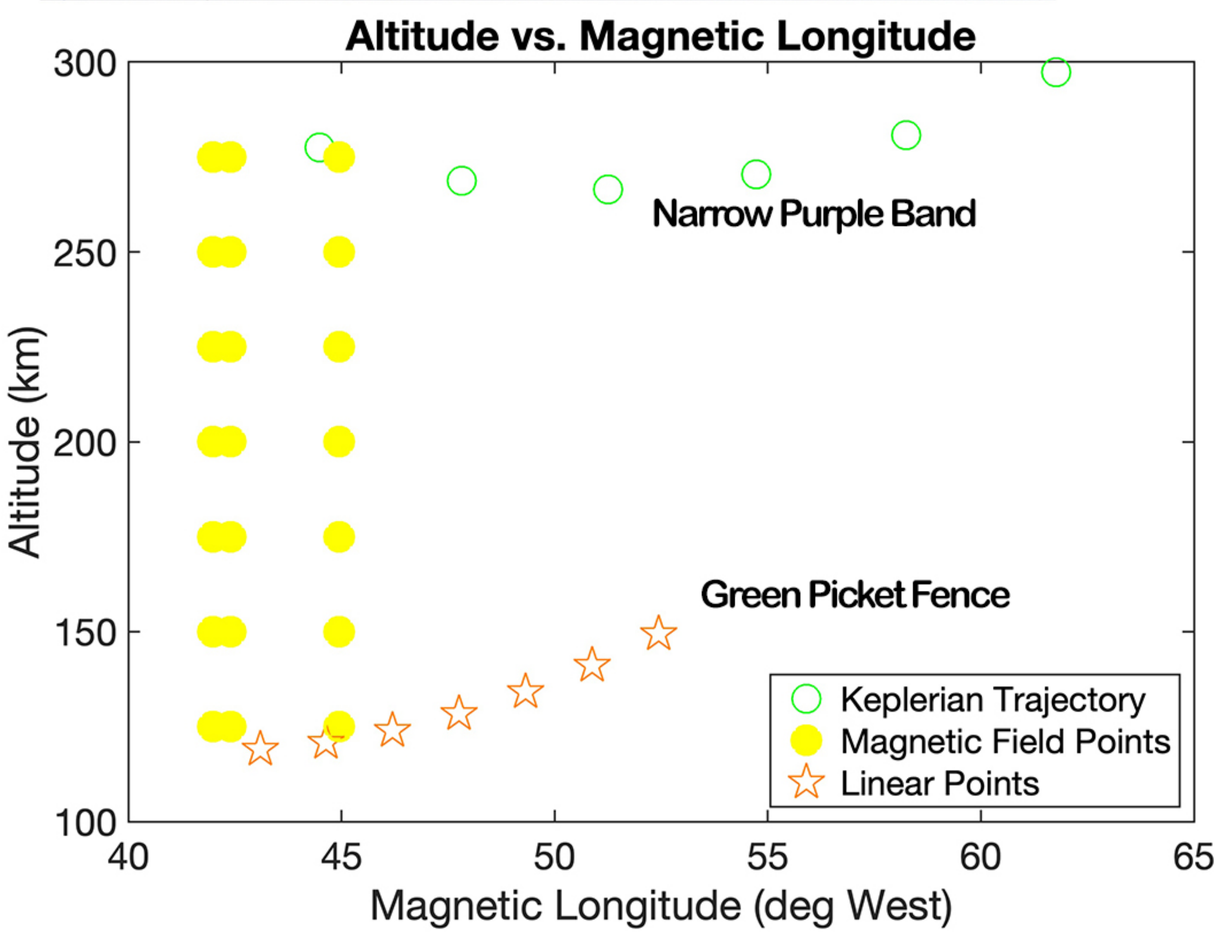

**Figure 7.**

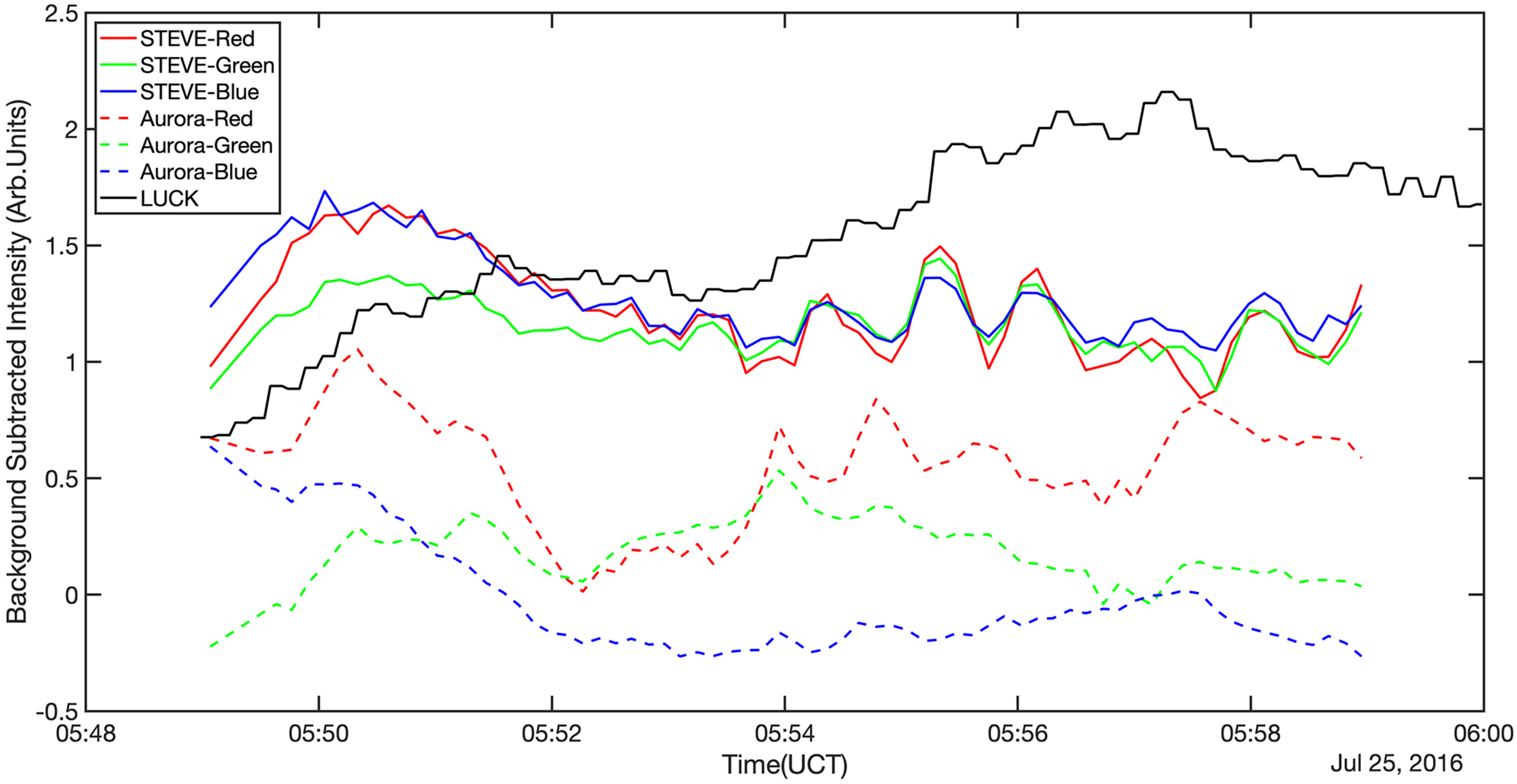
STEVE-Red
STEVE-Green
STEVE-Blue
Aurora-Red
Aurora-Green
Aurora-Blue
LUCK
Background Subtracted Intensity (Arb.Units)
2.5
2
1.5
1
0.5
0
-0.5
05:48
05:50
05:52
05:54
05:56
05:58
06:00
Time(UCT)
Jul 25, 2016

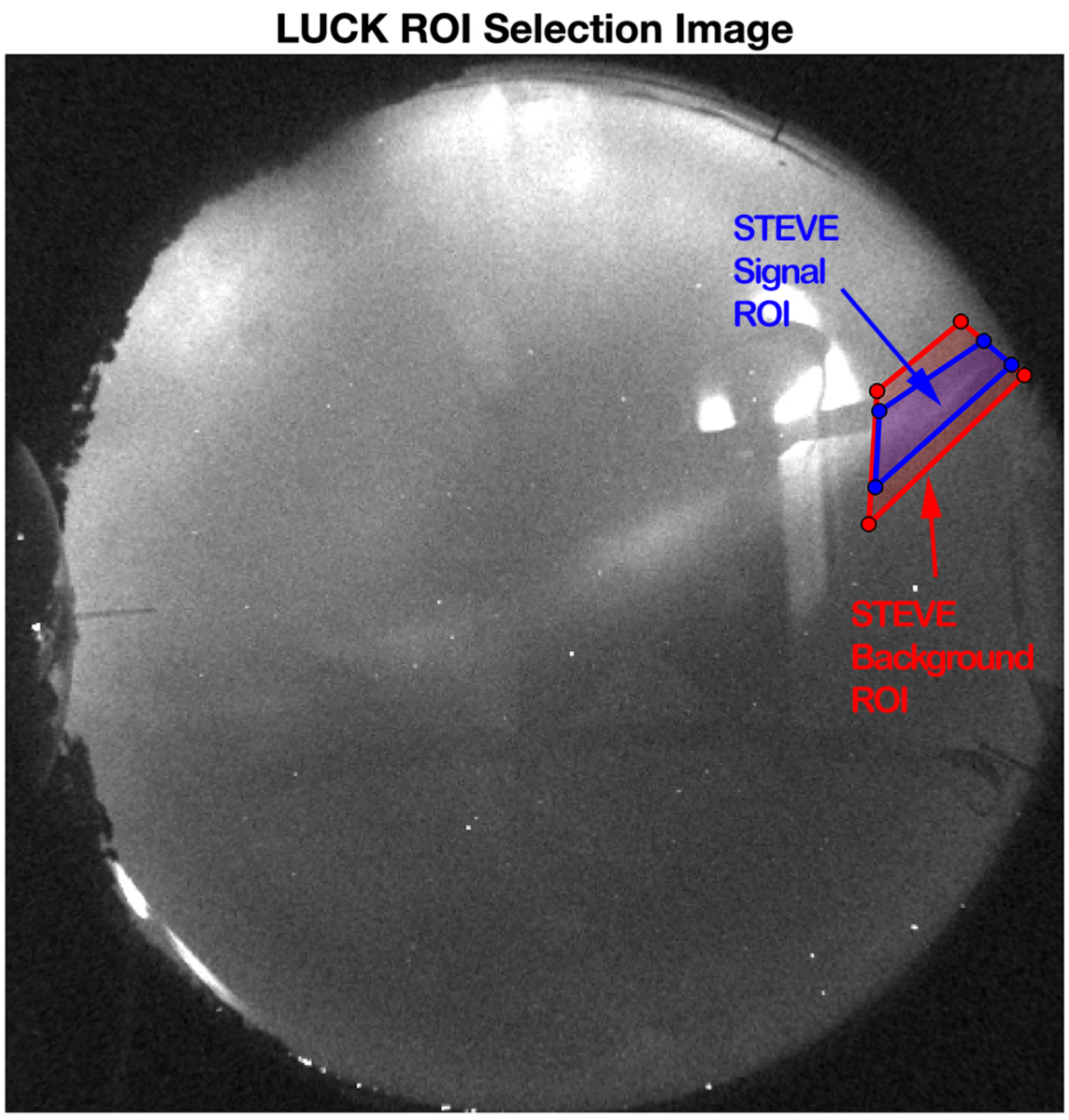
LUCK ROI Selection Image
STEVE
Signal
ROI
STEVE
Background
ROI

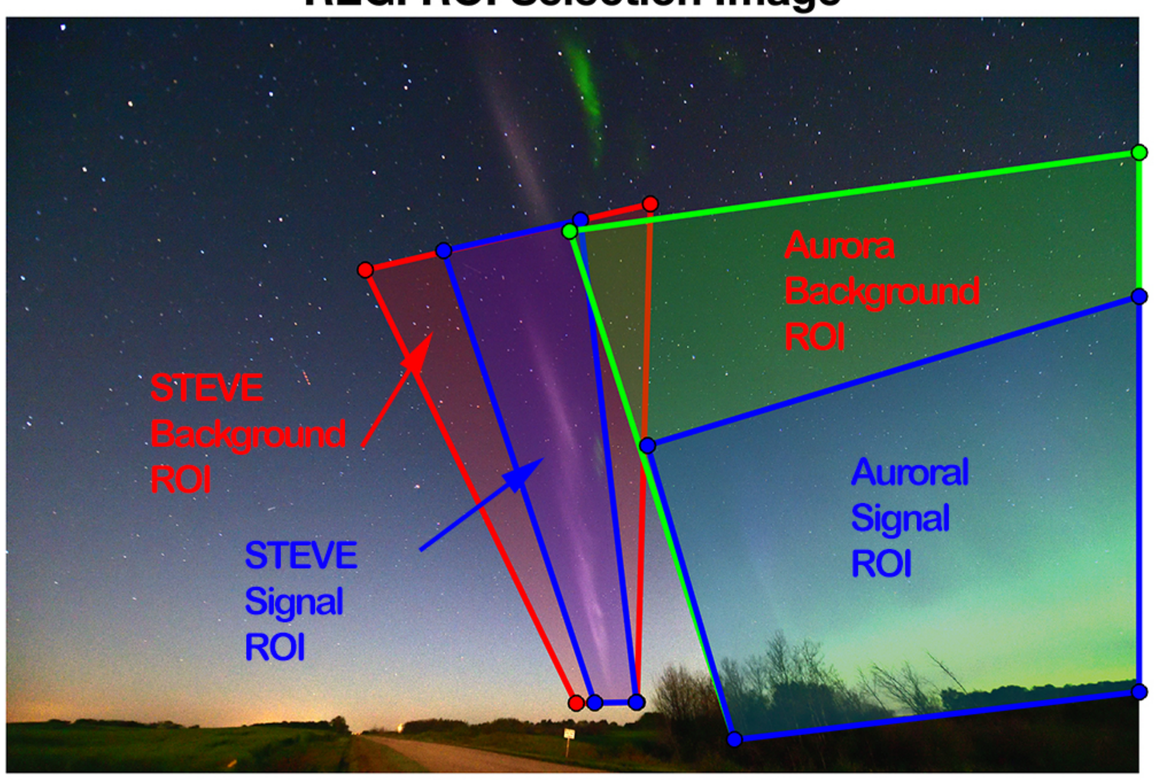
REGI ROI Selection Image
Aurora
Background
ROI
STEVE
Background
ROI
STEVE
Signal
ROI
Auroral
Signal
ROI